BACK TO BASICS: ON THE PROPER DETERMINATION OF FREE-SURFACE SLOPE (FSS)

IN GRADUALLY VARIED OPEN CHANNEL FLOWS

Emma House[a], Keyongdong Kim[b], Marian Muste[b], Ehab Meselhe[a], Ibrahim Demir[a]

[a] Tulane University: 6823 St Charles Ave, New Orleans, LA 70118, U.S.A., ehouse@tulane.edu, emeselhe@tulane.edu, idemir@tulane.edu.

[b] University of Iowa: IIHR-Hydroscience & Engineering, C. Maxwell Stanley Hydraulics Laboratory, Iowa City, IA 52245, U.S.A., kyeongdong-kim@uiowa.edu, marian-muste@uiowa.edu.

Corresponding Author: Emma House ehouse@tulane.edu

Abstract

This study is a fundamental evaluation of the fluvial wave propagation in river reaches affected by hysteresis, one of the most complex open-channel topics, materialized in loops and lags among hydraulic variables. Hysteresis processes are still understudied as measurements in natural streams for the whole wave propagation duration are hardly available, while the data from existing gaging sites (almost exclusively relying on stage-discharge relationships) can deviate up to 65% from the actual flows. A better understanding of hysteresis in general and its impact on streamflow monitoring in unsteady flows can be obtained if the free-surface slope (FSS) is determined and analyzed for its variation during wave propagation. Reliable FSS replication in such flows requires a robust understanding of the spatial-temporal sampling constraints. The study addresses the basic, but still weakly resolved, issue of tracing the FSS for waves of different magnitudes and durations. We do so by translating theoretical concepts on oscillatory waves to fluvial counterparts and observing rules for sampling continuous-time signals with discrete-time measurements. The conceptual understanding is verified with numerical simulations and experimental data represented in Eulerian and Lagrangian observation frameworks. We demonstrate that sampling stream stages with spatial and temporal resolutions (expressed in terms of fractions of the wavelength, dx_i/λ_R, and duration, $\Delta T_i/T_R$ for the flood wave to reach its peak) between approximately $0.0075 \leq dx_i/\lambda_R \leq 0.01$ and , $0.004 \leq \Delta T_i/T_R \leq 0.06$, respectively, are required to properly trace FSS for subsequent usage in experimental or numerical simulation contexts.

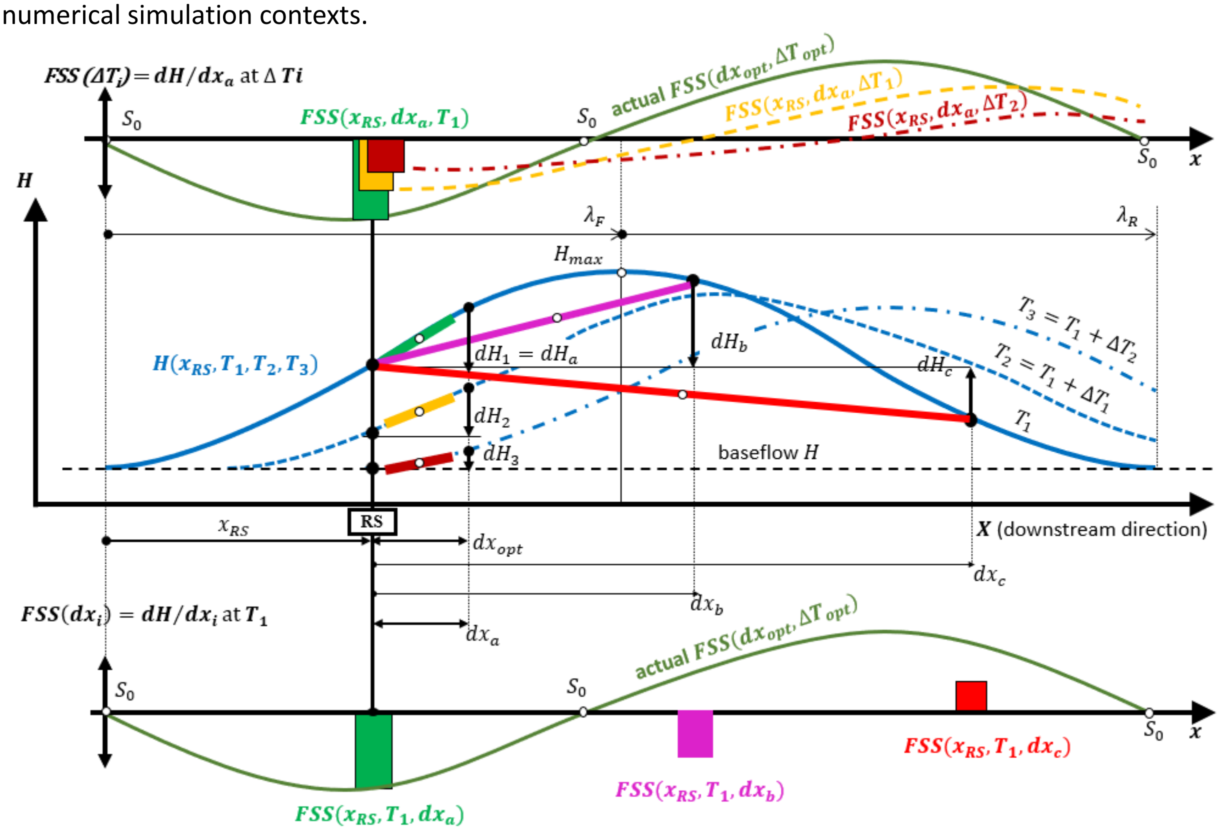

Proper selection of the spatial-temporal resolution for the determination of free-surface slope (FSS) is critical for the accurate reconstruction of the flood wave shape (traced by water surface elevations - WSE) as well as for capturing the FSS changes during the fluvial wave propagation. An increase of the distance used for determining the free-surface slope (i.e., decreasing the spatial resolution) and/or of the time interval between the WSE samples (i.e., decreasing the temporal resolution) result in a deterioration of the accurate tracing of these important variables for streamflow estimation.

Key Words: Free-surface slope (FSS), Gradually varied flow, Open-channel flow, Hysteresis, Streamflow monitoring, Wave propagation, Spatial-temporal sampling.

1. Introduction

Hydrologists routinely measure water-surface elevation (a.k.a. stage) or index-velocity (acquired at a point, along a line, or over a plane) to convert these data into much-needed streamflow records for supporting critical investigations supporting water resources management and research. The conversion is made via empirically constructed rating curves (RC) that typically require multi-year data collection depending on the local geomorphological conditions, drainage basin size, and frequency of flood events. The direct and continuous stage and index-velocity measurements acquired at the site and the pre-constructed ratings are assembled in the stage-discharge (labeled HQRC) and index-velocity (labeled IVRC) monitoring protocols that are globally applied for continuously providing streamflow at a river cross section (Rantz et al., 1982; Levesque & Oberg, 2012; Muste et al., 2020). In contrast, the estimation of the free-surface slope (FSS) over a channel reach are, by far, less frequently captured than stage and index-velocity measurements, as these data have typically been used to complement the HQRC method. One role played by FSS measurements is to improve the accuracy of the stage-discharge rating in higher-range flows where direct measurements for rating construction are not as dense as in the lower range. This indirect method for computing discharges is labeled as slope-area (SA) and assumes a quasi-steady flow regime in the channel (Dalrymple & Benson, 1984). The assumption implies that the discharge is constant over the reach where the FSS is measured.

Another traditional use of the FSS is for adjusting the simple HQRC for flow unsteadiness and non-uniformity effects, as it is widely recognized that this method is inaccurate in these flow regimes (Holmes, 2016). The adjustments require the development of additional empirical or semi-empirical relationships covering the whole range of flow occurring at specific stream gaging sites (Jones, 1916; Rantz, 1982; Kennedy, 1984). The rating adjustment approaches carry different labels depending on how the free-surface slope is measured, determined, or used (Schmidt, 2002; Schmidt & Garcia, 2012). Some of these approaches are criticized for their weakly posed physical foundations (e.g., assuming time-wise steady flows for describing unsteady flows and/or simplified wave types during flood propagation) and the statistical approaches applied to the raw data (e.g., Fenton & Keller, 2001). The above FSS-based estimation methods have typically been developed around mechanical and electrical pressure sensors submerged in the water column (Freeman et al., 2004; Turnipseed & Sauer, 2010). Using FSS as the main variable led to the revitalization of the slope-area method in a continuous monitoring method (e.g., Smith et al., 2010; Muste et al., 2019) and enabled short-term forecasting using a data-driven approach (Muste et al., 2022). The main objective of this paper is to deep dive into the requirements for properly sampling stage in space and time to accurately determine FSS.

Why is there a renewed interest in determining the free-surface slope? The proliferation of a new generation of stage sensors with lower installation and operation costs and acceptable accuracy in the last 50 years has led to a variety of alternatives for continuously measuring stages at two or more locations with the purpose of determining FSS (Smith, 2003; Kean & Smith, 2005; Cordova, 2008; and Clayton & Kean, 2010). This approach of indirectly measuring discharges is labeled Continuous SA (CSA). Initially developed by the U.S. Geological Survey to calibrate and validate numerical models for ephemeral streams (Smith, 2003, Cordova, 2008), nowadays the CSA method is tested as a superior and cost-efficient monitoring alternative to the HQRC method. While modernized versions of the pressure sensors continue to be used for estimating FSS for obtaining discharges (e.g., Mrokowska et al., 2015a; Stewart et al., 2012), new measurement principles are increasingly being tested. These new instruments determine water elevation non-intrusively using microwave (Chen et al., 2023), ultrasonic (Pereira et al., 2022), radars (Fulford, 2016), lidars (Paul et al., 2020, Wickert et al., 2024), close-range imagery (Noto et al., 2022; Manfreda et al., 2024), or airborne (satellite) interferometry (Schumann et al., 2010; Altenau et al., 2016).

Taking advantage of the availability of new generation sensors, scientists have expanded the use of FSS estimations in conjunction with more or less complex governing equations for steady, uniform flows (Smith et al., 2010; Muste et al., 2018; Frasson et al., 2021; Wickert, 2024) as well as for unsteady, non-uniform flows (Arico et al., 2009; Perumal et al., 2007; Dottori et al. 2009; Muste et al., 2025). The former group of FSS-based methods uses energy or Manning equations in various arrangements (i.e., direct usage based on "flow-law" parameters as formulated in Frasson et al., 2021, or power-law relationships as in Wickert, 2024). The second group uses the Saint-Venant equation commonly applied for simulating unsteady shallow water flows under various assumptions and approximations (Dottori et al., 2009; Triki et al., 2014; Triki et al., 2017; Muste et al., 2025). The latter group accounts for the hysteresis effect, a complex flow process property especially important during unsteady flow progression in flood-prone lowland rivers materialized by "loops" and "lags" between flow variables during the propagation of fluvial waves. Hysteresis is inherently neglected by the HQRC method and incompletely traced by the IVRC and CSA methods (Muste et al., 2020). Multiple studies show that estimating the FSS is critical in capturing the fluvial wave dynamics for river sites prone to hysteresis (e.g., Fenton, 2001; Aricò et al., 2009; and Dottori et al., 2009). The FSS can be determined by using stage measurements at two cross sections (Equation 1) or by converting the FSS time-derivative measured at a location in conjunction with analytical relationships.

$$FSS = \frac{(WSE_{US} - WSE_{DS})}{\partial x} \tag{1}$$

Given the limited reliance on the data resulting from conventional streamflow monitoring during unsteady and nonuniform flows, there is a perceived need for simultaneously measuring multiple hydraulic variables that are subsequently ingested in shallow-water equations for mass, momentum, and energy conservation (Muste et al., 2025). We use the multiple variable term herein as the widely used stage-discharge monitoring method ingests only the continuously measured stage for creating time series. We are currently exploring a new monitoring method using this approach, where the instantaneous FSS and its variation in time are essential for the method's implementation. The novel method, labeled Hybrid Streamflow Monitoring System (HyGage), aims at eliminating or reducing the reliance on the effort- and time-expensive rating curves by using various forms of the flow governing equations in conjunction with direct measurements of the hydraulic variables and their derivatives sampled with high-spatial-temporal resolution (NSF, 2022; NOAA, 2023). The novel method is currently under testing for monitoring purposes with ad-hoc data publicly available (Muste et al., 2025) and has proven promising for supporting streamflow forecasting (Muste et al., 2022). During HyGage development, we have found limited information regarding essential aspects of FSS. This paper aims to fill some gaps in our knowledge and capabilities to determine in-situ FSS.

The paper is organized as follows: We first explore definitions for the free-surface slope determination for various types of waves and subsequently analyze the impact of the change in spatial-temporal resolution on the FSS estimations with illustrations generated with numerical simulations and in-situ measurements. A discussion of other factors involved in the measurements and determination of FSS and light guidance for practical applications close the paper.

2. Research Questions on FSS Determination

The published literature covering FSS data reports slope values determined from water surface elevations acquired over a wide range of distances, from several tenths of meters (Smith et al., 2010) to tenths of kilometers (e.g., Dottori et al., 2009; Schumann et al., 2010). In fact, recommendations for simulations exist (Moussa and Boquillon, 1966) but similar guidance for field measurement does not.

Lacking uniform guidance driven by flow considerations, the decisive factor in selecting the FSS estimation locations are practical concerns related to capturing small water surface differences (e.g., 0.01 m for a 10^{-4} bed river slope) that can be distinguished from the uncertainties of specific measurement probes (e.g., less than 5%). Along these lines, Dalrymple & Benson (1984) recommend guiding the data collection “by one or more of the following criteria: a reach that is 75 times the channel mean depth, a fall in the free-surface equal to or larger than the velocity head, or a fall larger than 0.15 m.” ISO (2018) standard on slope-area method recommends a reach length that ensures a difference in water levels equal or greater than 0.25m. Fenton & Keller's (2001) recommendations are more restrictive: “As a rough guide, this might be, say, 10 cm, so that if the water slope were typically 0.001, they should be at least 100 m apart."

Dottori et al. (2009) advises that “… the distance between the two adjacent sections must be sufficiently small to allow for the constant flow rate assumption to be realistic, but at the same time it must be sufficiently large to allow the difference in water stage to be greater than the measurement instrument sensitivity and the water elevation fluctuations." These recommendations were formulated for ideal measurement situations whereby the river reach is not affected by geomorphological complexity (i.e., changes in the channel geometry or boundary roughness). Even in such idealized conditions, these heuristic approaches are insufficient for guiding the FSS estimation conducted in the ubiquitous flows associated with the propagation of fluvial waves, as they do not appropriately account for spatial-temporal flow changes, hence leading to unreliable results. The above recommendations rely heavily on judgements inferred from at-site measurements with little to no analysis to provide reasoning relevant to the physical processes governing open channel flow dynamics.

The issue of the spatial-temporal resolution required for calibrating and validating numerical models or accurately monitoring fluvial wave propagation becomes critical as the partial differential equations expressing the unsteady and non-uniform flows are applied to an elementary “lamina” of the flow, as illustrated in Figure 1. This elemental flow volume should be sufficiently small to fulfill the assumptions associated with the application of the elemental forces acting on it (Thomas, 1940; Chow, 1959; Henderson, 1966). These forces vary both in time and space, therefore, the changes in the flow variables driving them are expressed in terms of total and partial derivatives. As a consequence, estimations acquired in unsteady and/or non-uniform flows requires protocols that ensure that the data is “instantaneous” and "local”, i.e., small changes during data acquisition. An additional issue to be considered for FSS determination is regarding the most appropriate location to attribute the determined FSS value: at one end of the elemental volume or as the mean of corresponding quantities at the two volume ends. If all the above issues are resolved, the terms involved in flow governing equations such as the Saint-Venant equations (2-3) are satisfactorily defined.

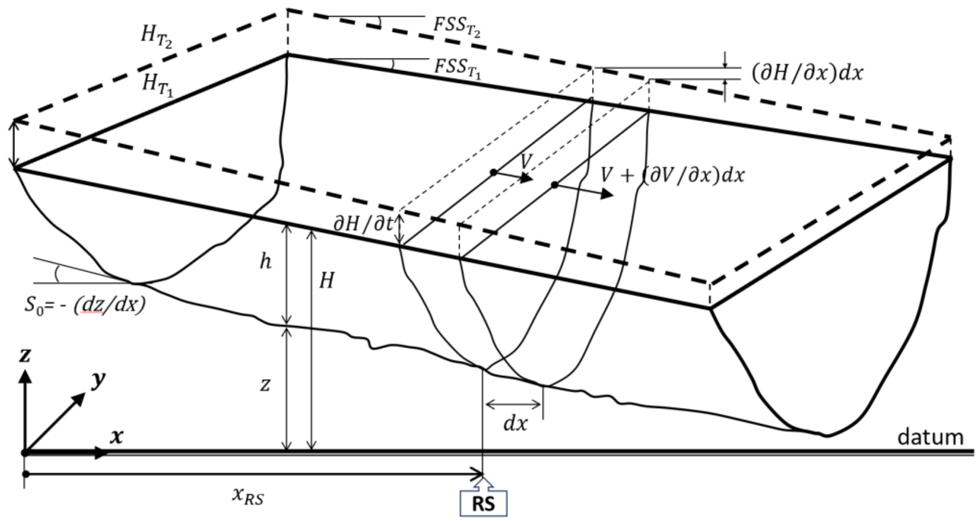

Figure 1. Definition sketch for the relevant terminology for FSS determination at a reference station (RS). Notes: i) the vertical scale is intentionally magnified to allow notation insertions; ii) the approximation $H = z+h$ is typically accepted for small values of the river slopes (Henderson, 1966; p. 90); iii) h is derived from H measurements, iv) $\partial H/\partial t \neq \partial h/\partial t$.

Given the practical difficulties in determining FSS estimations at desired specifications, the much-needed data for properly setting boundaries and initial conditions for modeling and monitoring unsteady flows is scarce and difficult to come by (Thomas, 1940). In most cases, the infinitesimal length and time intervals ∂x and ∂t (see Figure 1) are replaced by finite intervals, *dx*, and sampling times, *dt*, pending the availability of the data. Many works present differential equations in terms of "depth," which is an ambiguous and uncertain quantity, especially for natural streams, as the irregularities of the river bottom are typically unknown (Fenton, 2001). At times, the distances *dx* are those between successive gaging stations, and the sampling times, *dt*, can be anywhere from several minutes to 24 hours. Use of such coarse space and time intervals can introduce errors of considerable magnitude in the data provided for supporting model calibration and validation or when the data is directly used for monitoring or decision-making for real engineering problems.

The advanced measurement technologies available today (listed in the previous section) have the potential to overcome the coarse resolution of riverine measurement of the past by integrating high-frequency instruments that can measure simultaneously multiple variables with cost- and time-efficient deployments of higher density. Advanced computer-assisted modules offer a high level of automation for real-time data collection, processing, and communication (Sergeant & Nagorski 2015, Rode et al. 2016). Further enhancement of the spatial and temporal granularity can be expected by complementing the data collected at gaging stations with high-resolution digital terrain models acquired with airborne laser altimetry (Schumann et al., 2010) and with ad-hoc measurements or information garnered through appropriately screened citizen-science input (Nardi et al., 2022). The availability of these higher resolution spatial and temporal measurements enables additional clarifications regarding the protocols for data acquisition to make sure that important questions about in-situ FSS estimations are properly answered. Among the unresolved issues for FSS determination are: a) specifications on the optimal spacing between elevation sampling points (*dx*) and sampling rates (*dt*) for various flow regimes and flow transitions; b) specifications on the accuracy for FSS estimation with various technologies using rigorous assessments; c) evaluation of the viability of using slope estimations at one location in conjunction with analytical approximations of light numerical models (e.g., Aricò et al., 2009); and d) assessment of cost-effective practical methods to determine the channel bed slope that is needed to convert estimated FSS into flow depths (e.g., Isaak et al., 1999; Neesom et al., 2008). This paper aims at addressing the first issue listed above for the FSS determination using a generic framework relating flow mechanics, data acquisition and processing considerations.

3. Representativeness of FSS Determined with Various Spatial-temporal Resolution

3.1 Wave Characteristics

To address FSS sampling considerations, we approach fluvial wave propagation in waterways with terminology for oscillatory (periodic) water waves propagating in marine environments rather than using river hydrologic/hydraulic terminology. Both types of waves can be treated with the one-dimensional shallow water Saint-Venant equations as covered in hydraulics works (e.g., Henderson, 1966; Fenton, 2001) and in numerous advanced works on oscillatory waves (e.g., Keulegan, 1950; Lighthill & Whitham, 1955). While the latter approach is beyond the scope of the present discussion, we adopt the generic terminology for oscillatory waves with the intent to more rigorously describe fluvial wave propagation and subsequently apply robust criteria for its spatial-temporal sampling.

The generic description of the waves can be graphed as a function of time or space. The analogy between generic oscillatory and fluvial wave propagation in space coordinates is illustrated in Figure 2. A single-frequency (*v*) oscillatory wave of wavelength λ will appear as a sine wave, as illustrated in Figure 2a. The instantaneous amplitude of the wave is given by $\eta = P\sin(2\pi/\lambda)(x - ct)$, with notations for the equation terms given in the figure (Henderson, 1966). The inverse of wave frequency, *v*, is the wave period, *T.* The wavelength, celerity, and wave period/frequency are related by a purely kinematic relationship, $c = \lambda/T = \lambda v$, a useful relationship for representing the wave propagation. The speed of the wave depends on the properties of the medium (e.g., water column depth, wave amplitude) through which it propagates, and it is specific for each type of wave (e.g., small amplitude, cnoidal, or shallow water). The fluvial wave is a particular wave type characterized by distinctive features, as illustrated in Figure 2b (Henderson, 1966; Kozák, 1977): a) it is monoclinal (non-periodic), one-sided (i.e., oscillating only above the mean depth level) being produced by a single or superposed flow perturbation (e.g., runoff events), b) the shape of the wave is similar to a cnoidal wave (i.e., the rising stage duration is shorter than the falling stage) , and c) the wave becomes longer and lower as it travels downstream (i.e. wave attenuation) due to flow acceleration/deceleration and resistance.

a)

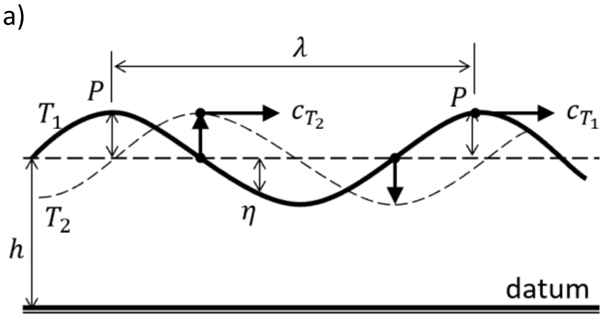

Notations (see also Figure 1):
H – free surface elevation
H – water depth
η – water surface elevation above the mean depth (wave amplitude)
P – maximum wave amplitude
c_T – wave propagation speed (celerity)
FS – free surface elevation
FSS – FS slope

b)

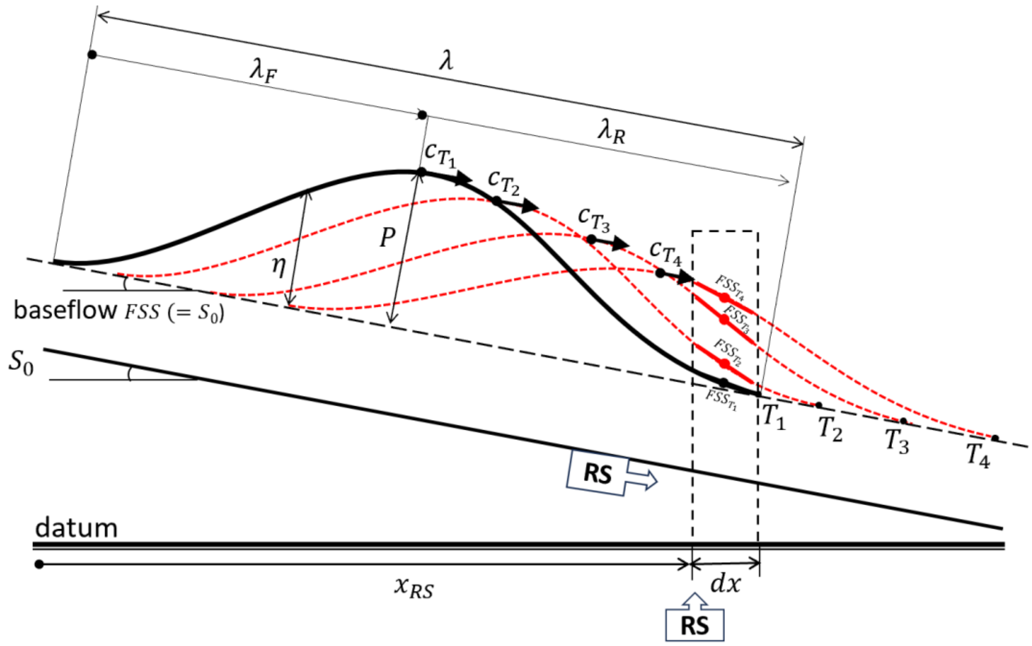

Figure 2. Definition sketch for wave characteristics: a) generic oscillatory wave, b) fluvial wave. Note: the vertical scale is intentionally magnified to allow notations.

3.2 Wave Sampling Requirements

The view of fluvial wave propagation using the generic oscillatory wave perspective facilitates implementation of the well-established rules for sampling fluid flow fluctuations as approached on in experimental fluid mechanics (e.g., Goldstein, 1996, and Muste et al., 2007). These rules stipulate that in order to accurately capture a fluctuation in the flow, the instrument's spatial-temporal resolution has to be commensurate with the fluctuation's spatial and temporal scales. For illustration purposes, consider first a stage probe placed in an idealized flow fluctuation represented by a periodic oscillatory flow (*ow*) of wavelength λ propagating with speed c (Goldstein, 1996). There are three criteria to fulfill to accurately trace flow oscillations. The first two criteria guide the selection of an appropriate probe (see Figure 3a), while the last criterion guides the operation of the selected probe (see Figure 3b). Short descriptions of these rules follow below:

C1. The probe size should be sufficiently small to resolve the spatial extent of the oscillation (i.e., its wavelength), which implies that the probe size must be less than $\lambda/2$ (the smaller, the more accurate sampling). This constraint ensures that there is no averaging of oscillation within the probe body (i.e., can be considered as local with respect to the oscillation's wavelength).

C2. The probe frequency response (the inverse of the time for capturing the signal) should be less than c/λ = (the smaller, the more accurate sampling). This constraint ensures that the probe does not sense a time-varying magnitude during the measurement (i.e., can be considered quasi-instantaneous).

C3. The sampling frequency during measurements (repetition rate of data acquisition), f_0, must be at least twice the frequency v of the smallest scale oscillation, c/λ_{min}. Criterion C3 is also known as the Nyquist criterion. This constraint ensures that the information on signal frequency is not lost during the acquisition and that the reconstruction of the oscillation shape in the frequency domain is close to the actual one.

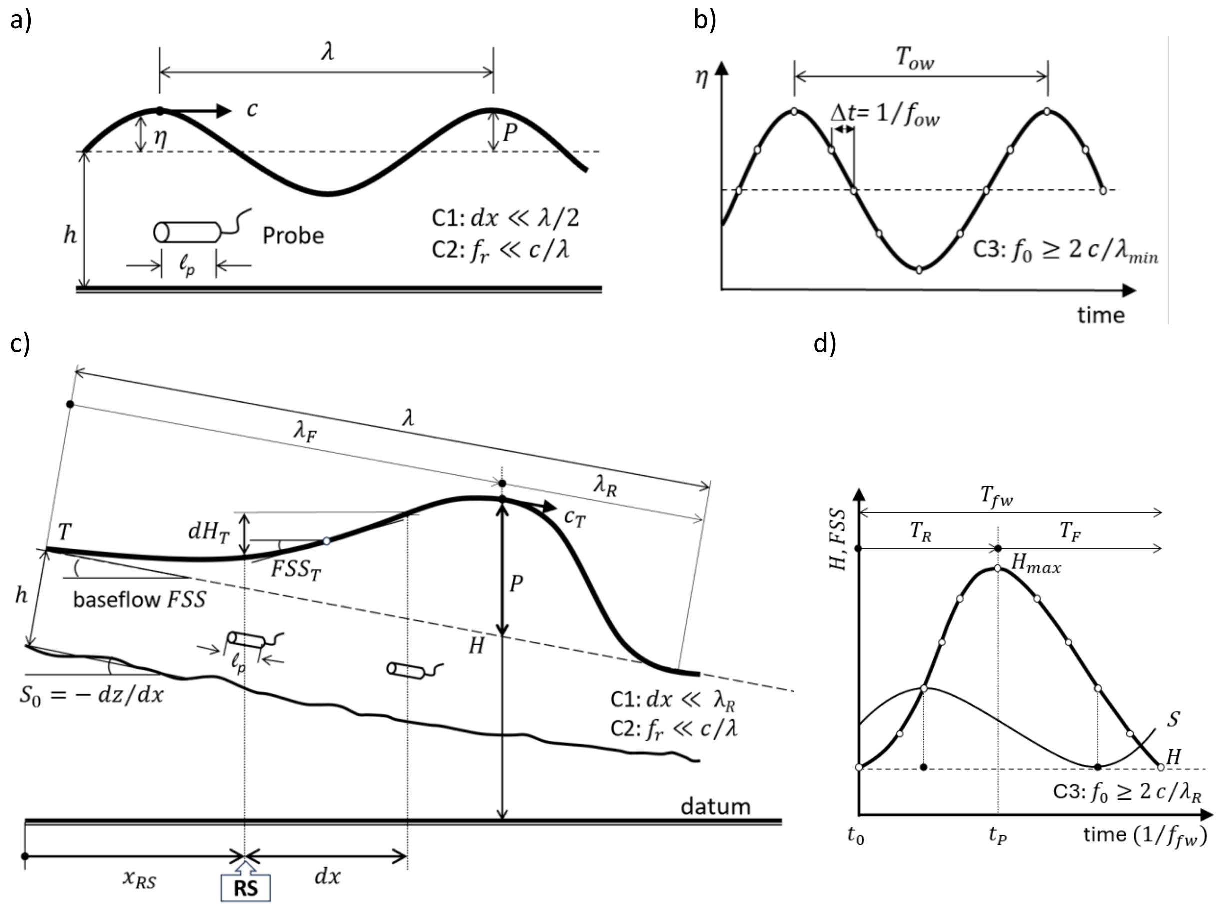

Figure 3. Constraints on the selection of instruments for sampling waves with proper spatial-temporal resolution: a) generic oscillatory wave, b) trace of the stage in time sampled with appropriate sampling frequency; c) fluvial wave; d) traces of the stage and FSS in time sampled with appropriate spatial and temporal resolution. Notations: f_r – probe frequency response; f_o – probe sampling frequency (= $1/\Delta t$, Δt – time between samples); λ – wavelength; λ_R – extent of the rising limb; λ_F – extent of the falling limb; T_{ow} – period oscillatory wave; T_{fw} - period oscillatory wave; l_p – probe length; Subscripts "*ow*" stand for oscillatory flows and subscripts "*fw*" stand for fluvial waves.

The above-mentioned measurement constraints applied to an oscillatory motion can be translated to the tracing of the fluvial wave (*fw*) propagation, which can be considered a special oscillation case (see Figure 3c). In the present discussion, the sampling rules need to be applied to two hydraulic variables: WSE and FSS, as the latter variable is determined using two or more stage probes. Essentially, accurate reconstruction of the spatial-temporal traces of the two variables requires the fulfillment of all three sampling criteria. The easiest criterion to attain accurate stage and FSS estimations is C2, as the water surface elevation in a cross section is made practically instantaneously with submerged conventional (e.g., pressure sensors) or modern non-intrusive (e.g., radar) probes. The priority in fulfilling the other two criteria is different for stage and FSS, even though the two variables are measured with the same "probes" because stage is measured at one location, while FSS is determined from stages measured at two or more distinct locations.

For sampling stages, the only practical concern is the fulfillment of criterion C3 as criteria C1 and C2 are typically achieved by conventional depth measurement instruments. Application of criterion C3 for fluvial waves takes the form: $f_0 \geq c/\lambda_R$, as typically the rising limb of the hydrograph, λ_R, is sensibly shorter (i.e., from 4 to 10 times) than the falling limb length, λ_F. This constraint can be easily accomplished with a variety of instruments sampling at a rate of several minutes as the fluvial wave propagation proceeds at slow rates of the order of several hours, days or even months. If this criterion is fulfilled, the trace of the wave in time coordinates is warranted. The trace of the wave in space is in question when sampled from a fixed point, as during the propagation of the non-kinematic waves, they are gradually attenuated and of a larger wavelength, as illustrated in Figure 2b.

The proper sampling of FSS, which is the focus of the present discussion, requires the fulfillment of criterion C1 in addition to C3, as the slope is determined from simultaneous stage measurements acquired at two or multiple cross-sections, as described in the first paragraph of Section 2. Fulfilling criterion C1 at a new measurement site poses some additional complexity, as the spectrum of fluvial waves possible at a river location and the individual wave characteristics might not be known when selecting the probe. For existing monitoring sites, an inspection of the historical records can indicate the magnitude of the flow events occurring at the site with a sufficient degree of accuracy for providing information for probe selection. There are two notable wave propagation features observable in Figures 2b and 3c that impact the FSS spatial sampling for flood waves. The first one is the flood wave decreases in height and (consequently) increases in length as it propagates downstream, as illustrated in Figure 2b. The second one is that the FSS values are larger on the leading part of a flood wave (i.e., rising limb) than the slope at baseflow whereas it is less than the baseflow slope on the trailing part (falling limb), as illustrated in Figure 3c. Figure 3d illustrates implementation of criterion C3 (i.e., sampling the stage and FSS with adequate sampling rate, Δt) to appropriately reconstruct the shape of the hydrographs for stage and FSS during the whole storm propagation event. Given that the FSS is steeper on the rising limb, Criterion C3 is related to λ_R.

4. Impact of FSS Sampling Strategy Selection

From this point on, the focus of our discussion is the impact of the sampling protocol selection and operation of the instruments for determining FSS during fluvial wave propagation. We approach this analysis first with numerical simulations applied to flood waves propagating in an actual river and experimental evidence collected on another river. The numerical study site is the Illinois River, a low-gradient bed slope river ($2x10^{-5} < S_0 < 3x10^{-4}$) that exhibits considerable hysteretic effects during fluvial wave propagation (Muste et al., 2022; Muste et al, 2025; House et al., 2024), hence the importance of accurately determining FSS is vital for streamflow estimation. In the subsequent discussion it is assumed that criteria C2 described above is fulfilled for both analysis alternatives as the FSS estimation duration is practically instantaneous with $f_r \ll 1/T_{fw}$ and the convergence of the simulation runs was also attained (see below).

We initiate the discussion with data produced by numerical simulations with the intent to replicate the flood wave with high fidelity and low noise in the variable traces, as well as allow reconstruction of the wave's FSS with a wide range of sampling rates (Δt_i of every few seconds or sampling intervals, dx_i along the channel reach as small as desired). This approach provides data far beyond the granularity offered by directly-observed data that are typically reported every 15 minutes and rely on stage measurements collected at large distances, typically between successive gaging station locations. In order to isolate the impact of the sampling strategy in space and time, we sequentially vary one resolution granularity at a time while keeping the other at an optimal value.

4.1 *Numerical Simulations Evidence*

The Illinois River simulations have been facilitated by the existence of a U.S. Army Corps of Engineering's model used for the Upper Mississippi River Flood Management study (USACE, 2022), with the extents shown in the map in Figure 4. This modeling case study was carried out using the 1-dimensional HEC-RAS modeling software (Brunner, 1997) that realistically simulates fluvial waves in long, prismatic channels while respecting the continuity and full dynamic equations (2-3) for the wave propagation, thus approximating well the water surface (i.e. free-surfaces).

$$\frac{\partial Q}{\partial x} + \frac{\partial A}{\partial t} = 0 \tag{2}$$

$$\frac{\partial Q}{\partial t} + \frac{\partial (QV)}{\partial x} + gA\left(\frac{\partial z}{\partial x} + S_f\right) = 0 \tag{3}$$

where *Q* is discharge, *A* is cross-sectional area, *V* is average velocity, *x* is distance along the channel, *t* is time, *z* is water surface elevation, *g* is the gravity constant, and S_f is friction slope.

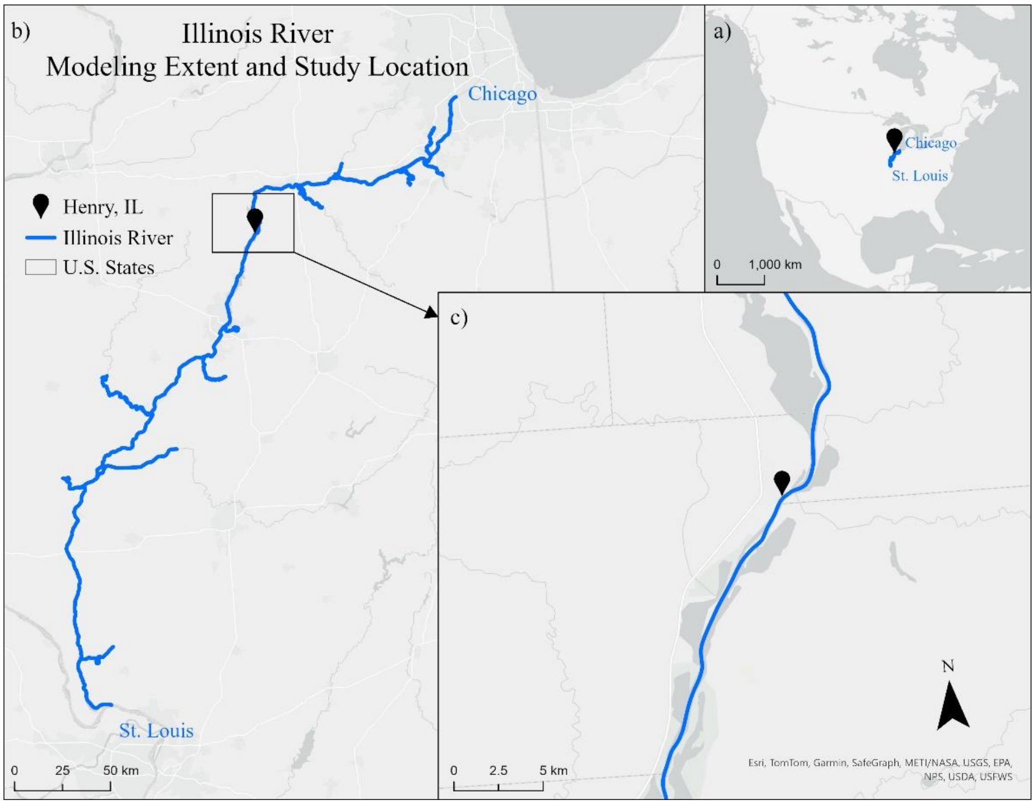

Figure 4. An overview map: a) North America, b) the Illinois River RAS model extent with the monitoring station case study location, and c) Henry, IL case study location inset map.

Use of the real-world and detailed complexity of the USACE model is however not the best option for the present analysis as it adds unwanted "noise" to the free-surface slope sampling analysis due to the presence of multiple bridges, bed-slope changes, and channel expansions/contractions altering the flow path. Moreover, when we examine the whole 252-long river mile reach from Marseilles Lock and Dam (near Chicago) to the Mississippi River at Grafton (near St. Louis), the flood wave produced by a major runoff event can be clearly resolved for only several short time steps. Additionally, with the low-gradient bed slope and large variation in water levels, when we examine this type of observed or simulated data, it is difficult to discern the FSS changes in the way we are interested in this study.

Instead of using the real-world modeling approach, we opted to reduce the complexity of the channel geometry for a clearer exploration of FSS sampling issues and to isolate the unsteady flow effect from other possible complexity factors. Since the full Saint Venant equations are used to simulate the flow for both the actual and simplified geometries, we are assured that all aspects of the flood wave are represented, and we may explore wave shape and water surface slope precisely. The reduced complexity model was set up using the Henry (IL, USA) average channel characteristics (i.e., a constant bed slope of 0.00027, 450 m width, and a Manning roughness coefficient of 0.025) over a straight, rectangular channel geometry, 80 km long river reach. This way, the model is representative of the Illinois River at Henry, IL, and is long enough to reach a converged solution. The simulated stage and streamflow hydrographs and stage-discharge rating curve are determined to adequately represent the reality of the hysteretic system, through the reduced complexity modeling and validation methods described in House et al. (2024).

For the present analysis, we simulate a synthetic hydrograph with the goal of observing the entire flood wave within the spatial window of the modeled reach. Thus, we can create profile plots such as in Figures 6, 7, and 8b, to study the entire fluvial flood wavelength for a given timestep. The modeled synthetic flood event replicates an April-May 2019 storm with normal depth at the downstream boundary, but is set up with a drastically reduced timestep and accordingly 10% of the flow rate to emulate a more flashy rainfall event and meet the desired profile parameters. We adjusted the reach length and hydrograph shape until a reasonable hysteretic flood wave was simulated. To ensure the credibility of the numerical model simulations, a sensitivity analysis was performed until a solution independent of the spatial-temporal resolution was obtained. For this purpose, we gradually changed the model *dx* and *dt* until the numerical model produced output independent of the resolution of space or time step (Thompson, 1992). The iterative process is illustrated in Figure 5, where the 150 m and 30 seconds spatial and temporal resolutions used for running the simulations are practically overlapping on the simulations run with *dx* = 300m and *dt*= 1 min. The simulation model convergence is considered for the present analysis equivalent to fulfilling Criterion C2 for accurately sampling the hydrographs.

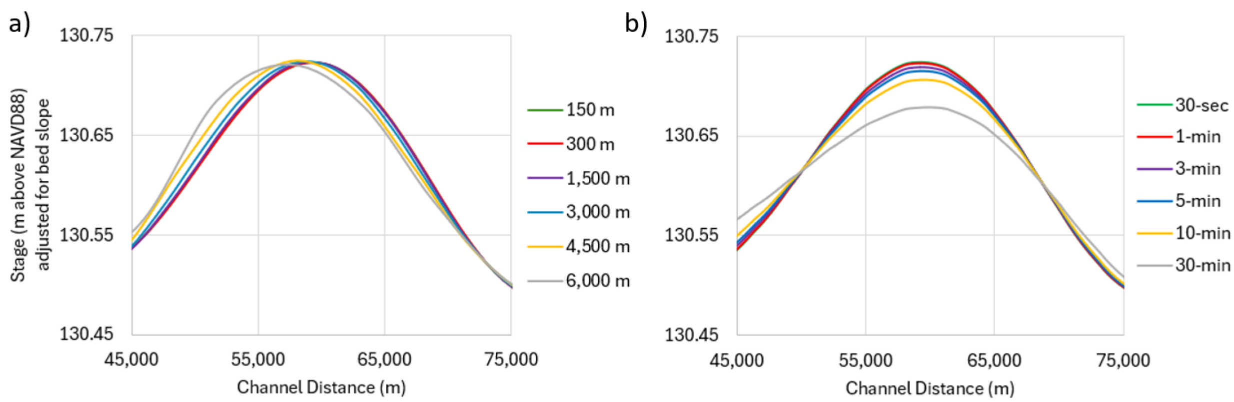

Figure 5: The reduced complexity model water surface profile produced by varied a) spatial resolution with *dt*=1-min and b) computational intervals with *dx*=300 m. The smallest space and timestep solution plotted (green) are hidden under the converged solution lines (red).

The bottom plot in Figure 6 compares the shape of the selected flood event propagating along the stream and the FSS estimated at various times (i.e., *T1, T2, T3*) using a Lagrangian wave representation framework (i.e., the observer moves with the wave). The FSS is determined using the stage measurements acquired from a fixed Reference Station (RS) and another downstream location at distance *dx*. Ensuing from the convergence analysis presented in Figure 5, the sampling criteria C2 and C3 are fulfilled (i.e., ensuring that the shape of the wave is accurately reconstructed in space and time). Under the assumption that the operation criterion C1 is also valid, the expected trend of the estimated FSS follows the line indicated by the continuous green line shown in Figure 6 top. Note that FSS is defined as -*dH/dx* to conform with conventional variable notations (i.e., Henderson, 1966). The actual FSS trend line can be obtained through on-site measurements if the smallest practically possible sampling distances, *dx,* and sampling rate, Δt (= T2-T1) « $1/f_{fw}$ are used (Criterion C3).

The ideal trend line for FSS shows that there is a phase shift between the stage and FSS peaks recorded at any instant (e.g., *T1, T2,* and *T3)* and that there are three fixed points where the FSS value is equal to S_0, (situation corresponding to a steady and uniform flow condition): at the beginning and end of the propagating wave duration and at the FSS inflexion point located close, but not identical with the location of H_{max} as explained in Muste et al. (2025). Another observation on the bottom plot in this figure is that the FSS value estimated over the same distance *dx* from the RS is different during the wave propagation because the slope is captured on different wave phases due to its downstream movement and wave attenuation. The combined effect of these two factors produces a decrease of the determined FSS if the time between samples is much larger than indicated by criterion C3.

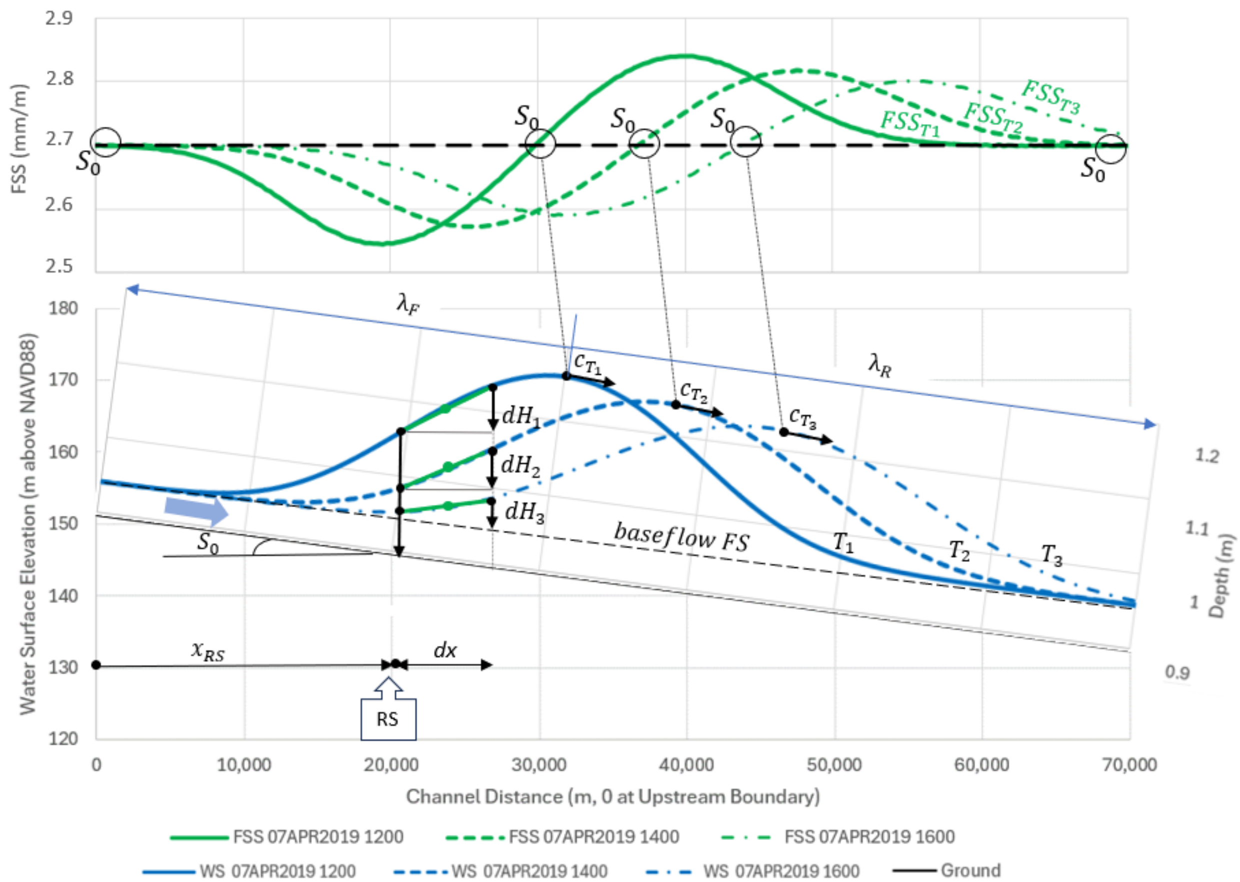

Figure 6: Simulated wave shape and FSS progression in space (Lagrangian view) captured at three-time steps 2-hours apart (Lagrangian representation framework).

While Figure 6 illustrates important aspects of fluvial wave propagation and of the associated FSS trendline, it does not directly address the sampling resolution aspect that this paper has as its main goal. In Figures 7-9, we explore how the determination of FSS changes with different spatial-temporal stage sampling intervals. For this purpose, one sampling parameter (i.e., *dx* or *dt*) is incrementally varied while the other is retained at the smallest resolution, nearest-optimal, value. For instance, in Figure 7 we explore the impact that varied distances between stage measurements have on the instantaneous determination of FSS. In the upper profile plot the continuous line substantiate FSS obtained with a single time step run with the converged model *dx*=300 m and *dt*=1 minute. The discrete FSS values (indicated by bars in the top plot) obtained by increasing the spatial sampling intervals for the stage measured at two locations using the same *dt* = 1 minute indicate a clear departure from the continuous line obtained with optimal sampling resolution. The illustrations in Figure 7 highlight that shorter spacing between stage measurements generally leads to more accurate local FSS estimation (i.e., better agreement between the FSS continuous line and the slope estimated for arrangements a, b, and c, than d, e, and f). Beyond the measurement arrangement c, the FSS estimates are considerably different from the continuous FSS line, hence inaccurately tracing the FSS realistic trend.

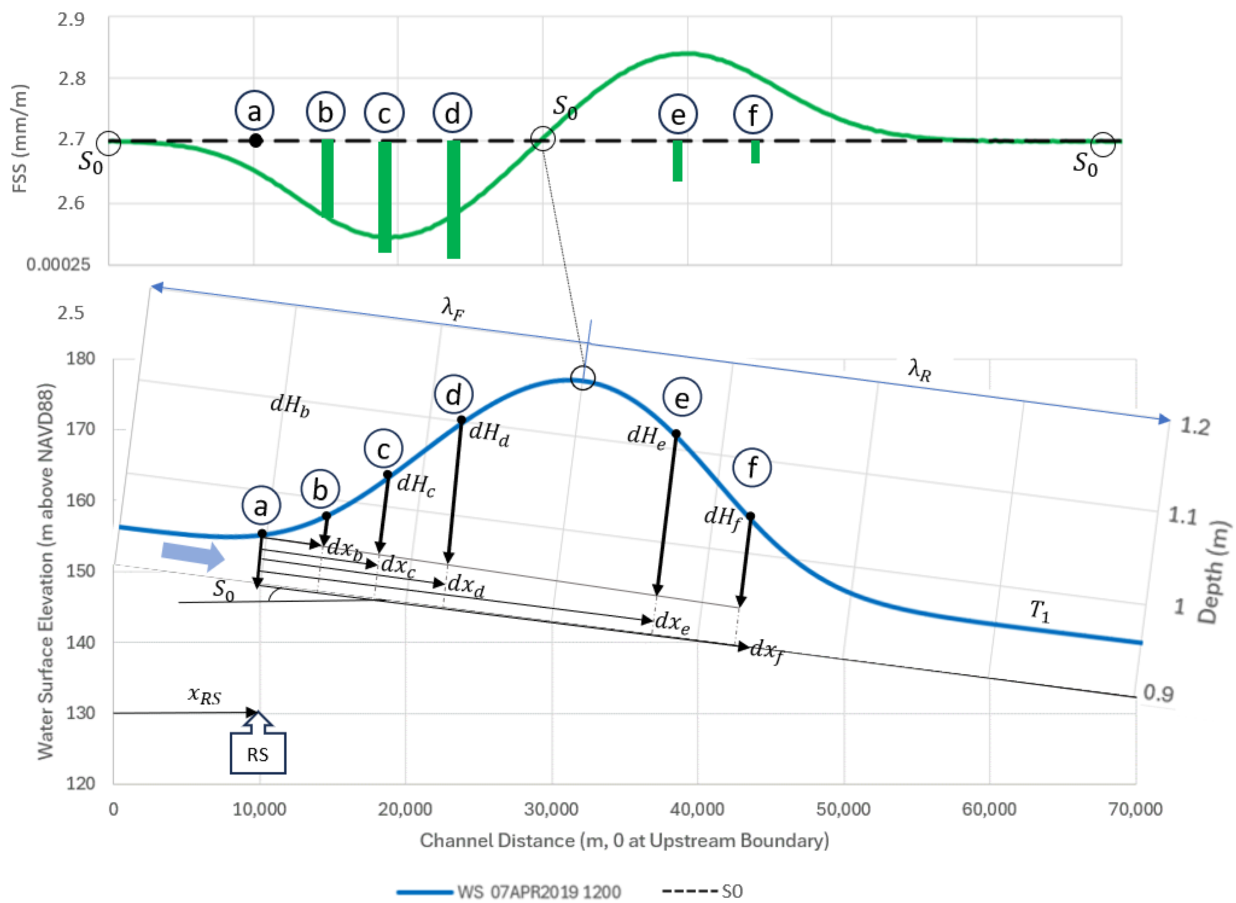

Figure 7: Simulated evidence using a Lagrangian representation framework of the impact of increasing the distance (d_{xi}) between the sampling points used for determining the FSS magnitude by keeping the sampling time constant (dt = 1 min) for all the tests.

Figure 8 provides an alternative view of the impact of FSS estimation with varied spatial sampling intervals for stage measurements (recall Equation 1). This analysis is obtained by sampling from a numerically simulated dataset converged at dx=300 m and dt=1 minute. The wave representation as observed from a fixed point (Eulerian view) illustrated in Figure 8a reveals a peak phasing between FSS and stage traces. This reconstruction of the wave is made first using a Eulerian representation framework akin to what is obtained when the observer is fixed and the wave shape is reconstructed from repeated observations of the stage (Figure 8a). The peak-phasing of streamflow variables follow the sequence: FSS peaks first, followed by the stage. This is also observed in the Lagrangian framework used for representing the fluvial wave in Figures 6 and 7. The lag between the peaks is site and event specific as illustrated analytically in Henderson (1966) and with field measurements in Muste et al. (2025). The shift between the peaks of the stage and FSS hydrographs is an intrinsic feature of hysteresis and can be used as a useful predictor variable for wave propagation forecast and streamflow routing as discussed in Muste et al. (2022).

In Figure 8, we further uncover trends seen in Figure 7 that collectively indicate the necessity of sampling FSS on short distances compared to the fluvial wave wavelength. Figures 8b and 8c complement the information shown in Figure 8a by illustrating the impact of increased time between samples using the Lagrangian representation of the wave. Too large of spatial intervals causes the sampling regime to "miss" parts of the fluvial wave, and result in a less accurate, diminished FSS value. The desired shorter distance between the adjacent sampling points used for determining the FSS, is however not always attainable as it is directly related to the resolution of the instruments used for the in-situ measurements. Specifically, since FSS calculation involves small and sensitive differentials, smaller distances between measurements points produce small slope values that cannot be easily detected from the scattering of the measurements acquired in field conditions. As discussed by Baydaroglu et al, (2024), the FSS data collected on short distances with conventional stage measurements are noisy, requiring extensive data smoothing procedures before obtaining FSS working values.

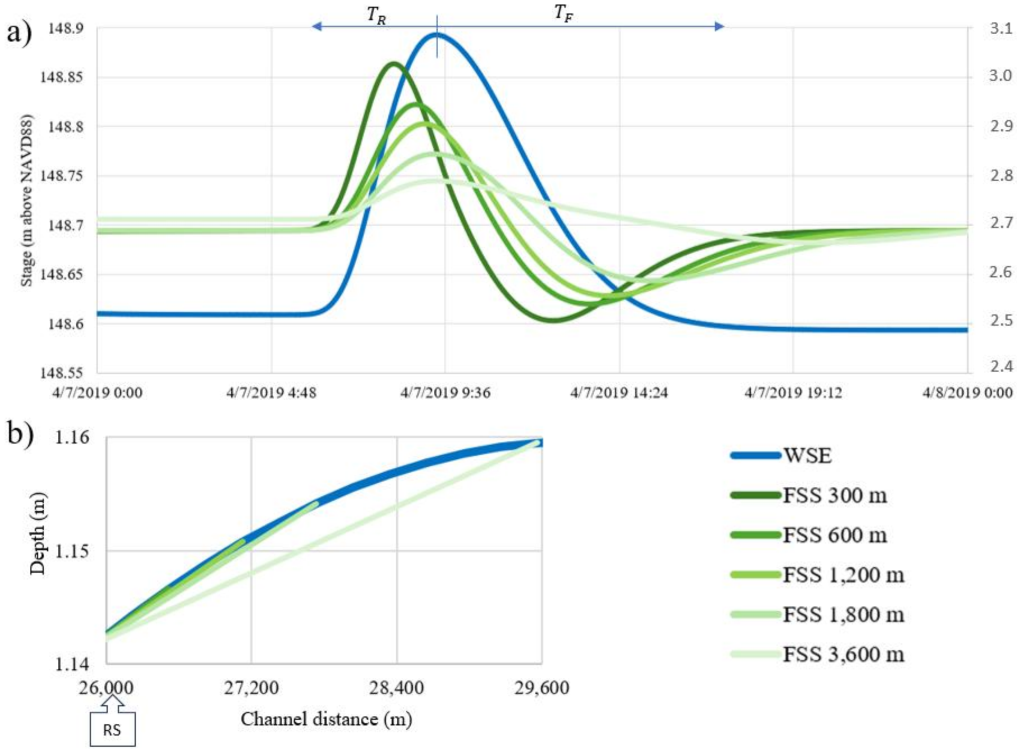

Figure 8: The impact of variable distance (d_{xi}) between the stage sampling points used for determining the FSS magnitude (Criterion C1) by keeping the sampling time constant (dt = 1 min) for all the tests. a) Eulerian representation framework; b) and c) Lagrangian representation framework.

Not only does increasing the distance between WSE sensors depreciate the FSS determination accuracy but a similar effect is observed regarding the temporal sampling. This is illustrated in the Eulerian representation framework in Figure 9 by decreasing the sampling resolution (i.e., increasing the time intervals between the sample acquisition from the order of minutes to days). The impact of the sampling rate with which the FSS is determined, akin to Criteria C3, is illustrated in Figure 9b where the larger times between samples lead to "missing" parts of the event propagation and causing the FSS values and trends to be incorrect (see Figure 8b).

As the color gradient becomes lighter with decreasing resolution in Figures 8 and 9, we observe depreciation of the stage hydrograph representation, and subsequently of the FSS estimates. Depending on when and where along the flood wave the measurements are made, the timing and magnitude of the stage and FSS estimations can be affected by large sampling intervals. The greatest errors are seen around the peak where the curvature of the graphs is pronounced leading to large differences, as highlighted in Figure 8b. Extremely large sampling intervals (i.e., decreased temporal resolution), as with the *dt*=1 day scenario in Figure 9, considerably distort the actual FSS values or miss the fluvial wave entirely.

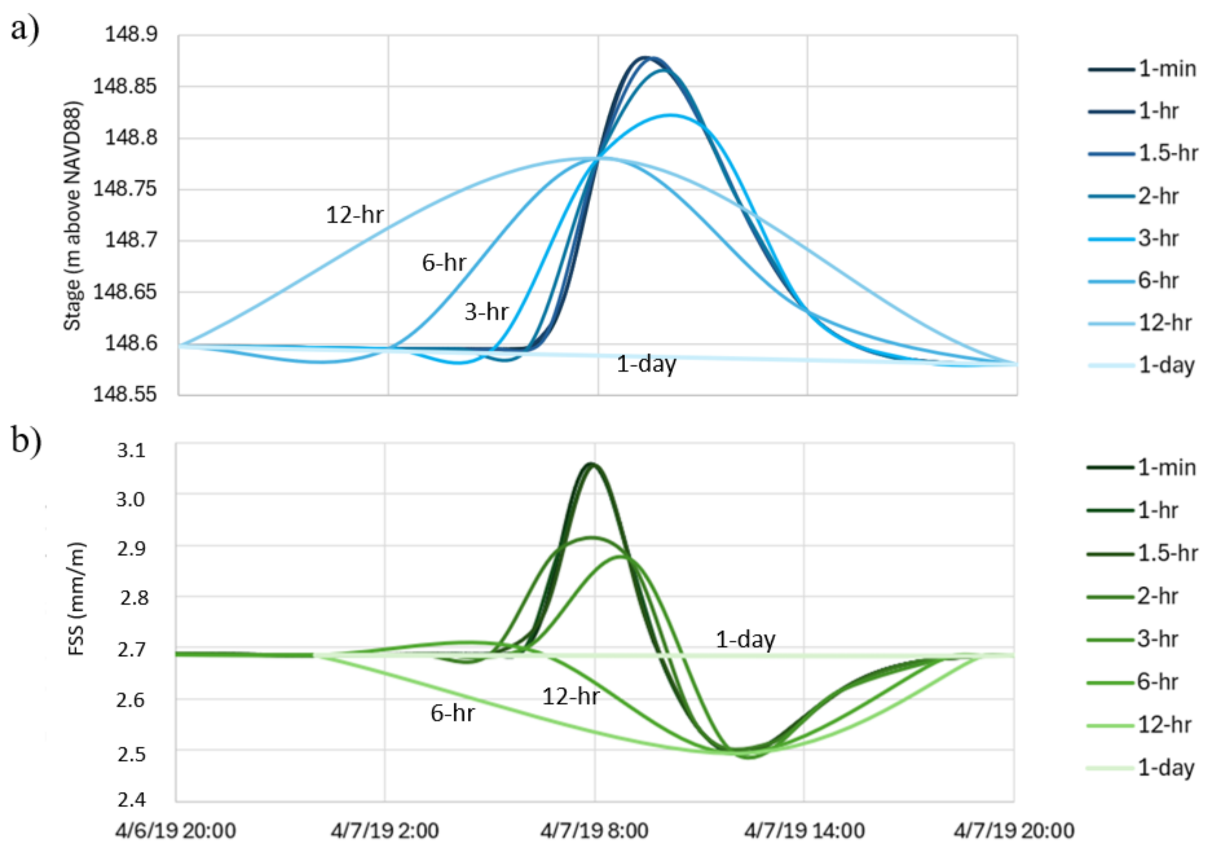

Figure 9: The impact of various sampling rates Δt from a numerically simulated solution with fixed *dx* = 300 m and a model *dt*= 1 minute (Criterion C3) illustrated in Eulerian representation framework: a) stage time series; and b) FSS time series.

4.2 *Experimental Data Evidence*

The FSS sensitivity analysis conducted on the numerical simulation results presented in Section 4.1 cannot be fully replicated with experimental data as no nearby stations with WSE measurements are available on the Illinois River. To our best knowledge, currently, there is no experimental evidence collected in situ to adequately support the sensitivity analysis on the FSS accuracy estimation as the costs and efforts of such studies are beyond the scope of typical projects. During the search for data at several hysteresis-prone sites, we identified several propitious experimental arrangements deployed on rivers in South Korea where the national hydrometric agency installed high-density monitoring stations with the desire to double-check the accuracy of individual gages within the streamflow monitoring network. One of these sites is the Naju gauging station (#5004550) on the Yeongsan River where a series of stations using stage-discharge rating (HQRC) and index-velocity rating (IVRC) are in operation, as illustrated in Figure 10a.

The Reference Station for the analysis of this river reach is HQRC1 (see Figure 10a) located on a bed slope of 0.00025 displaying a width of 150m and an aspect ratio (i.e., width/depth) of 36 at base flow. The range of flows recorded at this station varies between 526 m^3/s^{-1} and 7653 m^3/s^{-1}. The HQRC stations record continuous stages while the IVRC stations record continuous stages and index velocity (see Figure 10b). The sample event used for the present analysis occurred in 2020 (see Figure 10c). The time series for the stage and index velocity for the analyzed event at the IVRC1 station shown in Figure 10a are plotted in Figure 10d. Discharges at HQRC stations are obtained with stage-discharge ratings and with stage-area and index-velocity vs. mean velocity ratings at the IVRC stations. The protocols for constructing the ratings are similar to those used in the US (e.g., Kenedy, 1984 for HQRC and Levesque & Oberg, 2012 for IVRC).

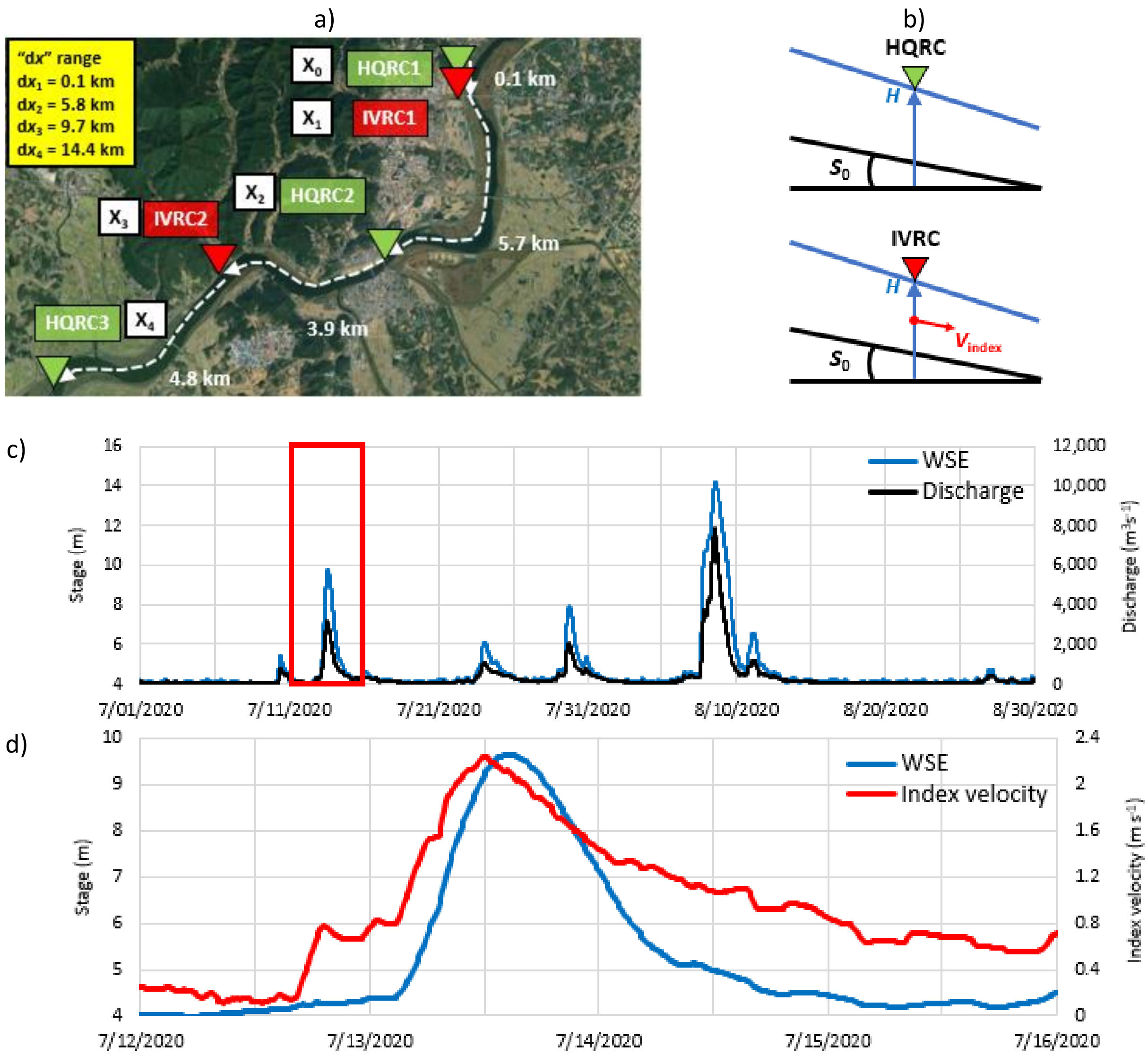

Figure 10. Stage-discharge (HQRC) and index-velocity (IVRC) stations sequentially located on Yeonsang River in South Korea: a) gaging stations layout; b) schematic of the measured variables at HQRC and IVRC stations; c) time series of stage and discharge for a reference period of 2020 and identification of

case study event; and d) traces of index velocity and stages at IVRC1 Naju gaging station for the cases study.

Taking advantage of the proximity of five stations located at relatively short distances apart (a rare layout in streamflow monitoring networks), the lack of inflows-outflows over the study reach, and the confinement of the flows within its leveed banks, we use the stage measurements acquired at consecutive stations for illustrating the FSS sensitivity analysis with the variation of the spatial-temporal resolution. The data provided by the cascade of stations on the Yeongsan River do not offer visualization capabilities on par with those of numerical simulations, as FSS can be only determined from the stage differences between the first station (HQRC1) and the downstream gages in a cascade of stations (IVRC1, HQRC2, IVRC2, HQRC3).

We illustrate the FSS sensitivity analysis to sampling distance, *dx,* and temporal sampling, Δt. Figure 11a displays the stage hydrograph at station HQRC1 along with the FSS determined over incrementally increased *dx* intervals of 0.1, 5.8, 9.7, 14.4-km long. The FSS plots in this figure are remarkably similar with to those illustrated in Figure 8a for analyzing the same sampling aspect with numerical simulations. The reasoning for the deterioration of the accuracy of FSS determination is clearly illustrated in Figure 11b by the Lagrangian representation of the stage in and the FSS values determined with simultaneous stage measurements at incrementally increased distances (similar to the simulated results shown in Figure 8b).

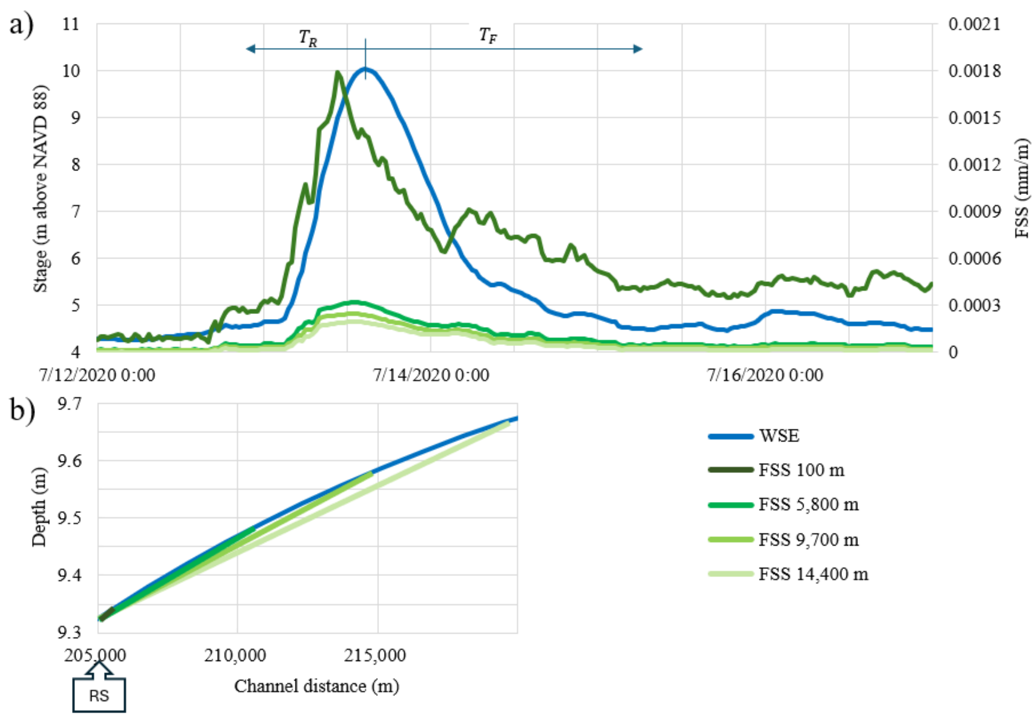

Figure 11. The impact of the sampling protocols for the reconstruction of the FSS time series: a) FSS determination with increased *dx* with HQRC1 as Reference Station using a Eulerian representation framework; b) FSS determination with increased *dx* with HQRC1 as Reference Station using a Eulerian representation framework.

While Figure 11 is an illustration of the Criterion C1 effects, the impact of the sampling rate for the reconstruction of the stage hydrograph and FSS determined for various rates is illustrated in Figures 12a and 12b, respectively. The last figures are illustrations of the impact of the Criterion C3 for sampling the FSS. Similarly to the inferences from Figures 9a and 10d with numerical simulations, one can notice a continuous deterioration of the FSS time series shape and continuous decrease of the FSS magnitude if the sampling times are incrementally increased.

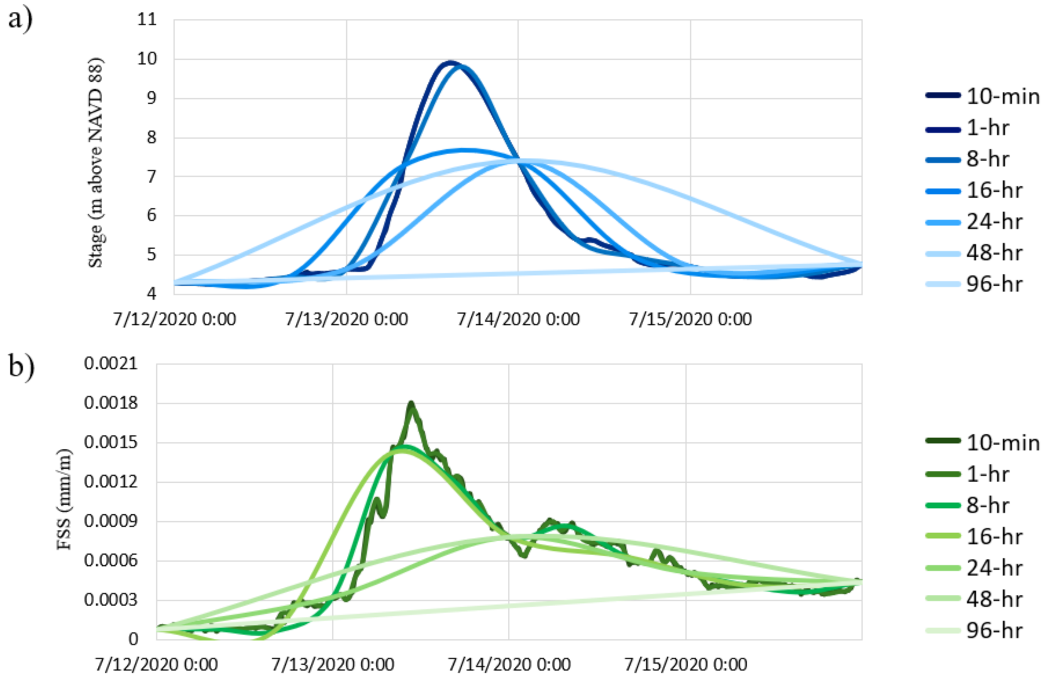

Figure 12. The impact of the sampling protocols for the reconstruction of the time series: a) stage reconstruction with increased sampling intervals, Δt, between the stage measurements at HQRC1 station; and b) FSS determination with increased sampling intervals, Δt, using simultaneous stage measurements at HQRC1 and IVRC1 stations separated by 100m.

5. Discussion

Throughout this study, we reconstruct FSS estimations during flood wave propagation using numerically simulated and experimental water surface data represented in Eulerian and Lagrangian perspectives. The conceptual fluvial wave tracing in connection with the spatial-temporal sampling resolution yields interesting results regarding the fundamentals of fluvial wave dynamics, worth detailed discussion and further exploration.

Ensuing from the considerations presented in Section 4, it is apparent that the FSS estimates decrease in magnitude (flatten) with low spatial-temporal sampling resolution, as parts of the waves, especially near their critical peaks, may not be accurately captured. These statements are well illustrated in Figures 8 and 9, where we observe depreciation of the captured stage hydrograph representation, and subsequently the FSS estimates, with lighter color gradient traces for decreasing spatial and temporal sampling resolutions. Depending on when and where along the flood wave the measurements are made, the timing and magnitude of the WSE and FSS determinations can be drastically affected by large sampling intervals. Specifically, larger spatial intervals can fail to capture small yet important shifts in wave behavior, which ultimately skews the overall FSS estimation (as in the Nyquist criterion and illustrated in Figure 8). The FSS signal is seen to depreciate with larger spatial sampling intervals due to the low-resolution sampling coverage. A similar effect is observed in Figure 9, where decreased temporal sampling resolution leads to missing wave dynamics and therefore inaccurate WSE and FSS reconstruction. Our findings are also supported by insights garnered through analyses applied to field measurements collected through previous studies (Morokowsa et al. 2015a, and Smith et al., 2010).

The illustrations in Figures 8 and 9 indicate that on the rising limb of the flood wave larger FSS values are observed crossing the bed slope value at the peak WSE, while smaller FSS values occur on the falling limb. However, the absolute deviation from bed slope is less pronounced on the falling limb than on the rising limb. These observations are indicative of the hysteretic flow propagation mechanics whereby the rising limb is more accelerated than the recession limb resulting in skewed shape of the fluvial wave, similar to the cnoidal waves (Henderson, 1966). Friction and diffusive forces play a larger role in the recession while acceleration terms are more active in the rising than the flood wave recession. This is well illustrated in Figure 6 with the earlier peaking of FSS, and as the water surface and FSS values continuously decrease as the fluvial wave propagates downstream.

Given that the slope is measured at two or more locations over a channel reach and that the cnoidal wave shape is not symmetric on the rising and falling phases, there is an additional aspect to be considered in the FSS estimation. This issue was addressed in a laboratory study conducted by Mokrowska et al. (2015b) where they compare the method used for calculating the slope over the reach, i.e., upwind, central, and downwind. Each of the three methods uses the FSS equation (1), only with different configurations of sampling locations. In the upwind approach, the estimated FSS is calculated from a Reference Station (RS) located at the downstream end of the reach, while for the central and downwind approaches the RS is located in the center and downstream end of the reach, respectively. The central approach requires at least three stage sampling locations. To illustrate the combined effect of the spatial resolution *dx* (Criterion 1) and of the location of the RS on the FSS estimation, Figure 13 assembles results obtained with numerical simulations applied to the case study event making distinction for the various phases of the wave propagation, i.e., rising, peak, and falling. Although dx close to zero is not meaningful for practical applications, we explore these scenarios to see the full spectrum of results according to the elemental volume concept. The analysis shows that the FSS values on the rising limb are larger than those on the falling limb for all wave phases. Also, the FSS values around the wave peak changes signs between rising and falling limbs (see Figure 13a and 13c) and settle close to the bed slope for the central estimation approach (Figure 13b).

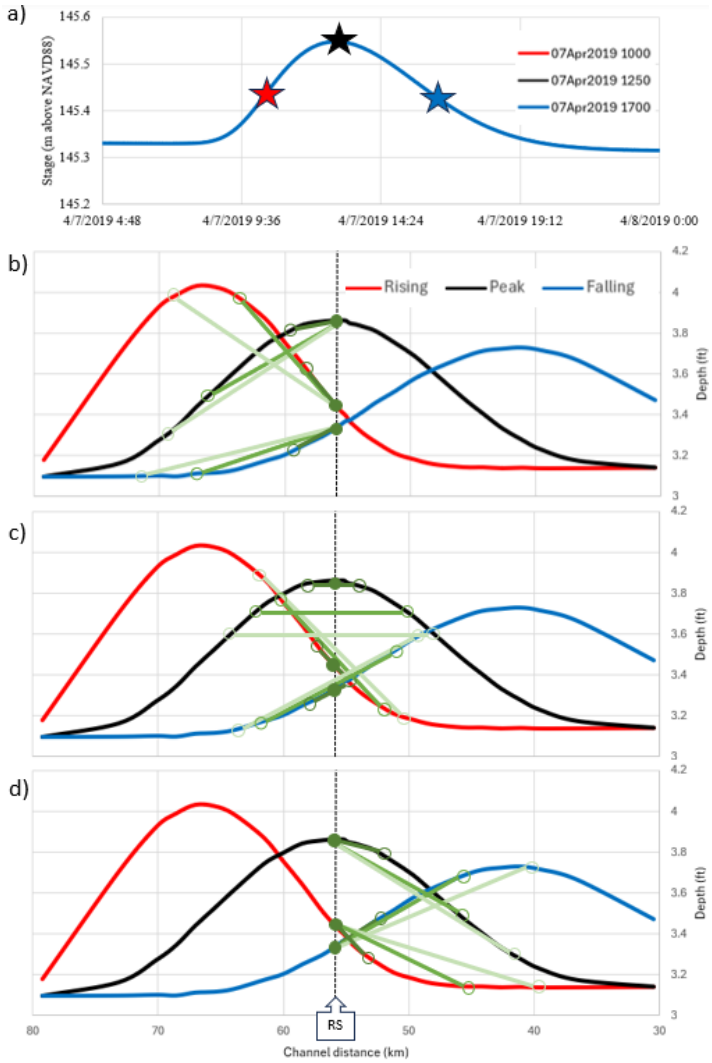

Figure 13: From a Eulerian (a) to a Lagrangian (b,c,d) viewpoint; depth profiles during various phases of the wave propagation relative to a station, and FSS estimation approaches with increased spatial sampling intervals (i.e, d_{x1} = 300 m, d_{x2} = 1,200 m, etc. per Table 1) based on the b) upwind, c) central, and d) downwind approaches. The a) hydrograph taken at RS depicts each time step we plot the depth profile corresponding to each phase.

Identifying the differences in the FSS traces for different estimation methods and phases of wave propagation requires a closer look into the numerical simulation. Figure 14 shows the cumulative effect of the spatial resolution with the sampling method in reconstructing the wave shape in a Lagrangian framework representation. Evidently, these sampling schemes are directly impacting the reconstruction of the FSS in the Eulerian representation. A common feature of the FSS estimation methods is a depreciating trend for FSS reconstruction with increasing *dx*. Besides this feature, each estimation method has a unique impact on FSS reconstruction. The central FSS calculation method exhibits the least depreciation with increasing *dx,* but ultimately, all three methods miss the wave entirely and estimate FSS values approaching the bed slope with very low spatial resolutions.

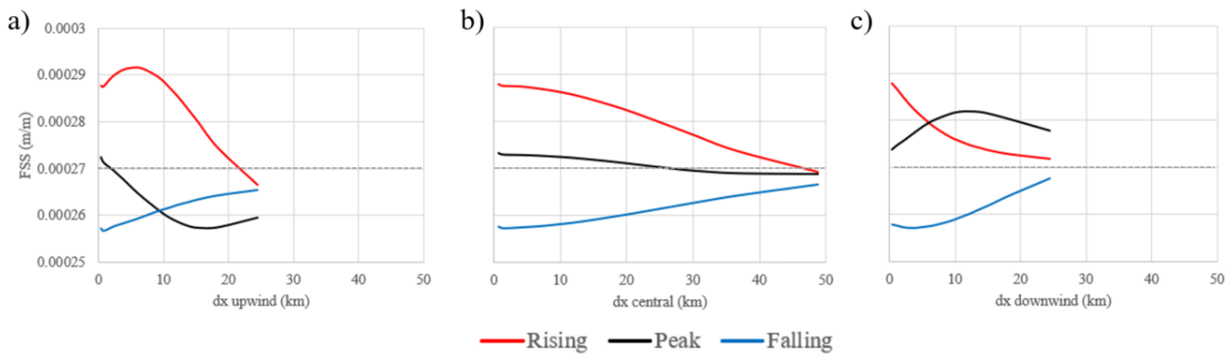

Figure 14. The simulated effect of the selection of spatial resolution, dx, and estimation approach for FSS estimation: a) upwind, b) central, and c) downwind. The bed slope is marked with a gray dotted line.

Elaborating further, Figure 15 illustrates the compound impact of the FSS estimation methods and the change in spatial resolution in reconstructing the FSS in Eulerian representation framework. Examining the impact of the upwind, downwind, and central FSS estimation methods within this framework (i.e., as time series) also reveals the depreciation of the FSS reconstruction with increased *dx*. Naturally, it can be noted that the timing and magnitude aspects of the FSS calculations are correlated: for example, in the upwind calculation highlighted in Figure 15b, larger dx means the FSS estimation peaks earlier, and thus, those values on the rising limb are overestimated, while those on the falling limb are underestimated. There is an disturbance to the captured FSS magnitude and timing with the selection of upwind and downwind methods, especially with large distances (Figures 15b and 15d), due to missing critical attributes of the wave propagation. However, there seems to be more temporal stability in the FSS calculation with the central method (Figure 15c).

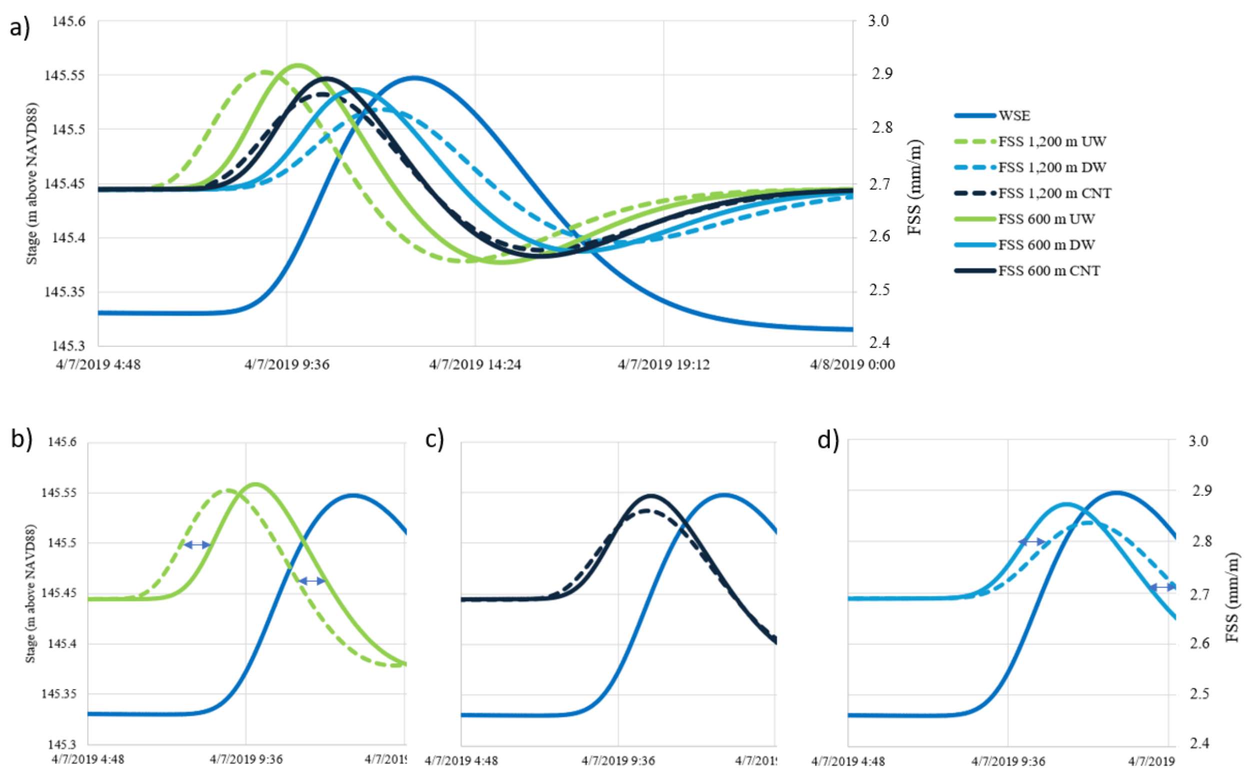

Figure 15: The simulated stage hydrograph with the estimated FSS time series for varying *dx* (solid line = 600 m, dotted line = 1,200 m) and FSS calculation method (green = upwind, blue = downwind, and black = central); a) all methods, b) upwind method, c) central method, and d) downwind method.

Given that fluvial waves display various wavelengths, amplitudes, and durations depending on the river characteristics at the monitoring site as well as the magnitude of the propagating wave (Muste et al., 2025), it is difficult to formulate generic ranges for the two sampling factors beyond the rough guidance offered by criteria C1, C2, and C3 described in Section 3.2. Using the analyses presented in this discussion, we can provide some illustrations of the order of magnitude for the sampling requirements relative to the wavelength and duration of the propagating waves, as shown in Table 1 with results obtained from numerical simulations and in Table 2 with data acquired in situ. It is important to note that experimental results come with inherent errors involved in the instruments, experimental protocol, and the fixed nature of sampling stations. Although the granularity of numerical simulations cannot be replicated, with the unique data from Naju, we can confirm general trends of the numerical findings.

Table 1: Summary of the impact of spatial and temporal resolution on the reconstruction of the actual FSS traces for the case study analyzed in Section 4.1.

Illinois River at Henry, IL synthetic storm event		
$\boldsymbol{\lambda_R}$ **= 40 km ,** $\boldsymbol{T_R}$ **= 4 hr (Figures 6 - 8)**		
Spatial resolution (dx_i)	**FSS Peak Reduction (%)**	
dx_1/λ_R = 0.0075	0	
dx_2/λ_R = 0.015	25	
dx_3/λ_R = 0.03	37	
dx_4/λ_R = 0.075	75	
dx_5/λ_R = 0.15	83	
Temporal resolution (Δt_i)	**FSS Peak Reduction (%)**	**WSE Peak Reduction (%)**
$\Delta t_1/T_R$ = 0.004	0	0
$\Delta t_2/T_R$ = 0.06	0.8	0.2
$\Delta t_3/T_R$ = 0.5	46	4.3
$\Delta t_4/T_R$ = 0.75	52	22
$\Delta t_5/T_R$ = 1.5	100	33
$\Delta t_6/T_R$ = 3	103	33
$\Delta t_7/T_R$ = 6	103	94

Table 2. Summary of the impact of spatial and temporal resolution on the reconstruction of the actual FSS traces for the case study analyzed in Section 4.2

<table>
<tr><th colspan="3">Naju 7/12/2020 ~ 7/16/2020 storm event</th></tr>
<tr><th colspan="3">λ_R = 115 km , T_R = 20 hr (Figures 10 - 11)</th></tr>
<tr><th>Spatial resolution (dx_i)</th><th colspan="2">FSS Peak Reduction (%)</th></tr>
<tr><td>dx_1/λ_R = 0.001</td><td colspan="2">0</td></tr>
<tr><td>dx_2/λ_R = 0.050</td><td colspan="2">82</td></tr>
<tr><td>dx_3/λ_R = 0.084</td><td colspan="2">86</td></tr>
<tr><td>dx_4/λ_R = 0.125</td><td colspan="2">89</td></tr>
<tr><th>Temporal resolution (Δt_i)</th><th>FSS Peak Reduction (%)</th><th>WSE Peak Reduction (%)</th></tr>
<tr><td>$\Delta t_1/T_R$ = 0.008</td><td>0</td><td>0</td></tr>
<tr><td>$\Delta t_2/T_R$ = 0.05</td><td>3</td><td>0</td></tr>
<tr><td>$\Delta t_3/T_R$ = 0.4</td><td>21</td><td>1</td></tr>
<tr><td>$\Delta t_4/T_R$ = 0.8</td><td>21</td><td>25</td></tr>
<tr><td>$\Delta t_5/T_R$ = 1.2</td><td>57</td><td>25</td></tr>
<tr><td>$\Delta t_6/T_R$ = 2.4</td><td>57</td><td>25</td></tr>
<tr><td>$\Delta t_7/T_R$ = 4.8</td><td>76</td><td>52</td></tr>
</table>

As illustrated in Figures 7-9 and 11-12, Tables 1 and 2 summarize the depreciation of FSS and WSE peak values with decreased spatial-temporal sampling resolution. The spatial interval $dx_i/\lambda_R \leq 0.01$ and temporal interval $\Delta T_i/T_R \leq 0.06$ setup yield satisfactory results for FSS estimates between two stage measurements, calculated with the upwind method. As suggested in Figures 13-15, the central method may have larger spatial resolution margins, with the depreciation of FSS taking longer.

As well as presenting confirmed findings from in-situ measurements, it is important to acknowledge the idealized nature of the numerical simulation results. The reduced complexity of the HEC-RAS model, with a rectangular channel and constant bed slope and roughness, does not mimic the complex conditions within natural rivers. Nevertheless, our results provide a solid, physics-based foundation for understanding FSS processes within a fluvial flood wave and offer guidance on the best FSS estimation methods. Natural rivers will have significantly more variability in the water surface thus the estimations of FSS may be far more variable and uncertain, especially at very small spatial intervals due to perturbations in the water surface. Nonetheless, the experimental evidence that we provide undoubtedly supports our numerical findings with these natural factors incorporated.

Although the two tables are in agreement in order of magnitude of depreciation, there is one important sampling factor, highlighted by the differences in FSS Peak Reduction trends between those in Table 1 vs. Table 2 and their corresponding Figures: the location of the sampling points relative to the propagation of the fluvial wave. For example, since the low resolution (i.e., $\Delta T_6 = 12$ hours) numerical simulation results captured one data point nearly at the negative peak of the FSS event, although the sampling of maximum FSS depreciates, the negative FSS peak was still captured (recall Figure 9b). In practice, achieving accurate peak estimates with large temporal intervals would be purely luck-based, so we need to rely on smaller, more confident, sampling intervals. At small sampling intervals, the choice of FSS estimation method becomes less critical due to the high spatial resolution capture of the flood wave. In this way, the upwind or downwind method can be used, and only two monitoring stations are required rather than three, saving time and funding resources.

In an attempt to guide the practical implementation of the present analysis inferences, it is anticipated that for typical mid-range conditions (a medium-size river located in lowlands exposed to a medium-size fluvial wave), the ideal interval dx_i for determining FSS is on the range of 300-500 m for the typical sampling time of up to 15 minutes used in current monitoring protocols. Besides the analytical wave sampling considerations formulated above, the selection of appropriate spatial and temporal resolutions also needs to account for instrument capabilities to accurately capture WSE sampled at one or more points. The precision of the instruments is continuously improved with the advancement of measurement technologies (i.e., enhanced instrument spatial-temporal resolution and sampling frequency) and the adoption of alternative measurement principles (e.g., the superior resolution of the lidar vs. acoustic instruments). For each measurement setting and instrument configuration, a balance must be struck between too large of an interval to capture an accurate magnitude/timing, and too small of an interval which introduces considerable noise due to the environment in natural systems and intrinsic instrument noise. By adopting optimal instruments and sampling regimes, even the minor dynamics of the flood wave can be captured, allowing for precise reconstruction of both the magnitude and timing of FSS and flood wave progression.

6. Conclusion

This study enhances our understanding of the fundamental properties of fluvial flood wave propagation characterized by interactions between flow dynamics. Unlike oscillatory waves, fluvial waves display unique behaviors due to hysteresis and evolving flow conditions, where free-surface slope (FSS) emerges as a critical variable. By examining FSS in both Eulerian and Lagrangian frameworks, we identified how these waves differ across propagation phases, revealing marked asymmetries between the rising and recession limbs, and characteristics sensitive to temporal and spatial changes in sampling. These insights bridge knowledge from oscillatory wave theory to natural fluvial systems, exploring what defines these unique waves and their inherent properties.

Our research underscores how spatial-temporal resolution significantly influences the accuracy of FSS reconstruction. Numerical simulations and field data highlight that reduced spatial-temporal sampling resolutions lead to notable declines in FSS estimation, as they fail to capture the intricate variations within each wave phase. The central differencing method shows robustness, retaining FSS timing even as spatial intervals increased, which is critical for tracking wave progression accurately. This is a unique opportunity because it means that, even with larger dx, we can rely on the crucial timing relationships between FSS and WSE with greater confidence, creating possibilities for monitoring and forecasting where finer resolution may not be feasible.

For river monitoring focused on the dynamic variable FSS, we recommend using the central method with a high temporal resolution and moderate spatial interval. For optimal results, we recommend using small ($dx_i/\lambda_R < 0.01$ and $\Delta T_i/T_R < 0.06$) spatial-temporal intervals in the sampling regime, and precise WSE instruments. These sampling requirements ensure accurate timing measurements and stability at even larger spatial sampling intervals. For the case studies analyzed in this paper, the practical recommendations indicate high-resolution stage sampling in the order of 300m-500m, and up to 15 minutes, respectively.

We argue that with current technology, high-resolution stage data can be collected to meet the Nyquist criteria and capture the flood wave FSS dynamics effectively. More advanced FSS protocol will lead to more accurate streamflow monitoring, notably in hysteretic streamflow by utilizing the CFSA and

HyGage methods. By establishing fundamental relationships and advancing precise monitoring strategies, this paper helps lay the groundwork for developing data-driven approaches in streamflow monitoring and forecasting. Our guidelines provide practical tools that address the nuances of FSS tracing in complex river flows, supporting flood risk mitigation and resilient water resource management. In this way, our work contributes to the evolving discipline of hydraulics, enhancing both theoretical and applied hydrology in the context of climate-impacted flood events.

Research Data

The data produced by this study (output from numerical models, experimental data, etc.) can be found in the following GitHub repository: https://github.com/ehouse25/FreeSurfaceSlope.

The data and software used for building and as input to the HEC-RAS model as boundary conditions are from publicly sourced databases:

- The United States Geological Survey (USGS) Water Data for the Nation via http://dx.doi.org/10.5066/F7P55KJN, http://waterdata.usgs.gov/nwis/ with public access conditions.
- The HEC-RAS model (software v6.1) used as the foundation of this study representing the complex IL River is preserved at USACE UMR Hydraulic Model Update webpage https://www.mvr.usace.army.mil/Missions/Flood-Risk-Management/UMRS-Hydraulic-Model-Update/, available upon request to Federal, state, local agencies, and NGOs along with their engineering consultants (USACE, 2022).
- Version 6.2 of the publicly available HEC-RAS software used for developing the reduced complexity models is preserved at https://www.hec.usace.army.mil/software/hec-ras/download.aspx, available via public access conditions.

Funding Sources

This work was supported by the National Science Foundation [Grant numbers NSF-EAR-HS 2139649 and 2139663]. The second author was supported by funding provided by the National Oceanic and Atmospheric Administration (NOAA), awarded to the Cooperative Institute for

Research on Hydrology (CIROH) through the NOAA Cooperative Agreement with The University of Alabama, NA22NWS4320003.

Author Contributions

Emma House: Numerical Investigation, Formal analysis, Writing – Original Draft, Writing – Review & Editing, Visualization. Keyongdong Kim: Experimental Investigations, Formal analysis, Conceptualization, Visualization. Marian Muste: Conceptualization, Methodology, Validation, Writing – Original Draft, Supervision, Project administration. Ehab Meselhe: Supervision, Project administration, Writing – Review & Editing. Ibrahim Demir: Supervision, Project administration, Writing – Review & Editing.

Vitae

Emma House: A Ph.D. student in the Department of River-Coastal Science and Engineering at Tulane University, Emma studies streamflow hysteresis to better understand riverine dynamics. Her research combines numerical modeling and data analysis to explore the processes driving streamflow hysteresis, with implications for improving flood monitoring and forecasting. Emma earned her previous degrees in environmental and water resources engineering from the University of Delaware. Passionate about applying her work to real-world challenges, she aims to contribute to advancing river science and enhancing climate resilience. Kyeongdong Kim: A postdoctoral researcher at IIHR--Hydroscience & Engineering, University of Iowa, Kyeongdong specializes in river hydraulics and hydrometric techniques. His research focuses on analyzing river flow hysteresis using water surface slope and aims to enhance the understanding of hysteresis effects in hydraulic processes. He has extensive experience in numerical modeling, GIS-based spatial analysis, and ADCP sensor-based field monitoring and data analysis. Kyeongdong earned his Ph.D. in Civil and Environmental Engineering from Dankook University, where he studied river flow patterns and flood wave propagation. His work aims to improve river monitoring and flood risk management through advanced hydrometric techniques. Marian Muste: Dr. Muste is Research

Professor with IIHR-Hydroscience & Engineering and Adjunct Professor in the Civil & Environmental Engineering Department at The University of Iowa. Dr. Muste's main areas of research is environmental river hydraulics, experimental methods, and instrumentation. He has conducted extensive investigations on the capabilities of acoustic instrumentation to monitor normal and extreme flows. He is lead editor for a recent book on Experimental Hydraulics and author or co-author of more than 250 peer-reviewed journal and conference papers and 75 technical reports. Dr Muste is hydrometry expert for United Nations Educational, Scientific and Cultural Organization and World Meteorological Organization.

Ehab Meselhe: Ehab Meselhe, Ph.D., P.E., is Professor in the Department of River-Coastal Science and Engineering at Tulane University. His research is focused on computer modeling of coastal wetland, estuarine, and riverine systems. He is particularly interested in integrating physical, ecological and social processes for inland watersheds riverine, deltaic and coastal systems. Ibrahim Demir: Ibrahim Demir is the Michael A. Fitts Presidential Chair in Environmental Informatics and Artificial Intelligence at Tulane University, Professor in the Department of River-Coastal Science and Engineering and a core member of the Tulane ByWater Institute. Leveraging cutting-edge artificial intelligence and data science, Demir develops innovative environmental information systems, notably creating early warning systems and digital twins for disasters. He leads the Hydroinformatics Lab, focusing on intelligent disaster analytics systems, augmented and virtual reality for environmental monitoring. Demir holds a PhD from the University of Georgia. He also serves as the Chair of the International Joint Committee on Hydroinformatics (IAHR/IWA).

Declaration of Interests

The authors report no conflict of interest.

References

Altenau, E.H., Pavelsky, T.M., Moller, D., Lion, C., Pitcher, L.H., Allen, G.H, Bates, P.D., Calmant, S., Durand, M. and Smith L.C. (2016). AirSWOT measurements of river water surface elevation and slope: Tanana River, AK, Geophysical Research Letters, 44 (1), doi.org/10.1002/2016GL071577, pp. 181-189.

Brunner, G. W. (1997). HEC-RAS river analysis system. Hydraulic reference manual. Version 1.0.

Chen, Z.;Wang, T.; Zhao, C.; He, Z. (2023). River Discharge Inversion Algorithm Based on the Surface Velocity of Microwave Doppler Radar. Remote Sens. 15, doi.org/10.3390/rs15194727.

Chow, V. T. (1959). Open channel flow. London: McGRAW-HILL, 11(95), 99,136-140.

Layton, J.A. and Kean, J.W. (2010). Establishing multi-scale stream gaging network in the Whiteware River basin, Water resources Management, 24, doi 10.1007/s11269-010-9624-x.pp. 3641-3664.

Cordova, J.T. (2008). Continuous Slope-Area Method for Determining Stream Discharge, poster presented at 2008 USGS National Data Conference.

Dalrymple, T. and Benson, M. A. (1967). Measurement of peak discharge by the slope-area method: U.S. Geological Survey Techniques of Water-Resources Investigations, book 3, chap. A2, p. 12.

Di Baldassarre, G., Schumann, GJ-P., & Bates, PD. (2009). Near real time satellite imagery to support and verify timely flood modelling. Hydrological Processes, 23, https://doi.org/10.1002/hyp.7229, pp. 799 - 803.

Dottori, F., Martina, M. L. V., and Todini, E. (2009). A dynamic rating curve approach to indirect discharge measurement, Hydrol. Earth Syst. Sci., 13, 847–863, https://doi.org/10.5194/hess-13, pp. 847-2009.

Dykstra, S. L. and Dzwonkowski, B. (2020). The propagation of fluvial flood waves through a backwater-estuarine environment. Water Resources Research, 56, doi.org/10.1029/2019WR025743, e2019WR025743,

Durand, M., Gleason, C. J., Pavelsky, T. M., Prata de Moraes Frasson, R., Turmon, M., David, C. H., et al. (2023). A framework for estimating global river discharge from the Surface Water and Ocean Topography satellite mission. Water Resources Research, 59, doi. org/10.1029/2021WR031614, e2021WR031614.

Fenton, J. D., & Keller, R. J. (2001). The calculation of streamflow from measurements of stage: CRC for Catchment Hydrology.

Fenton, J. D. (2010) The long wave equations, Alternative Hydraulics Paper 1, Available online at: http://johndfenton.com/Papers/01-The-long-wave-equations.pdf

Frasson, R. P. d. M., Durand, M. T., Larnier, K., Gleason, C., Andreadis, K. M., Hagemann, M., et al. (2021). Exploring the factors controlling the error characteristics of the Surface Water and Ocean Topography mission discharge estimates. Water Resources Research, 57(6), doi.org/10.1029/2020WR028519, e2020WR028519.

Freeman, L.A., Carpenter, M.C., Rosenberry, D.O., Rousseasu, J.P., Unger, R. and McLean, j. (2004). Use of submersible pressure transducers in water-resources investigations, Techniques of Water-Resources Investigations 8-A3, US Geological Survey, Reston, VA,

Fulford, J.M. (2016). Accuracy of radar water level measurements, in Manual on sea level measurement and interpretation, intergovernmental Oceanographic Commission, IOC/2016/MG/14 Vol5. Available online: https://pubs.usgs.gov/publication/70192079

Goldstein, R.J. (1996) Fluid Mechanics Measurements. 2nd Edition. Washington DC, Taylor & Francis.

Henderson, F.M. (1966). Open Channel Flow. Macmillan Series in Civil Engineering; Macmillan Company: New York, NY, USA, p. 522

Holmes, R. (2016). River rating complexity. Constantinescu, editor, River Flow, 10-14.

House, E., Meselhe, E., Muste, M., and Demir, I. (2024). Streamflow Hysteresis Analysis through a Deep Dive Budget of the St Venant Momentum Terms, Water Resources Research (Under Review).

Isaak, D.J., Hubert, W.A. and Krueger, K.L. (1999). Accuracy and precision of stream reach water surface slopes estimated in the field and from maps, North American Journal of Fisheries Management, 19(1), doi.org/10.1577/1548-8675(1999)019<0141:AAPOSR>2.0.CO;2, pp. 141-148.

ISO (2018). Hydrometry – Slope area method, 3rd edition. International Organization for Standardization, Geneva, Switzerland.

Jones, B.E., (1916). ”A Method of Correcting River Discharge for a Changing Stage,” Water Supply Paper 375, U.S. Geological Survey, pp. 117-130
Kean, J. W., and J. D. Smith (2005), Generation and verification of theoretical rating curves in the Whitewater River basin, Kansas, J. Geophys. Res., 110, F04012, doi:10.1029/2004JF000250.
Keulegen, G.H. (1950). “Wave motion”, Chapter 11 in H. Rouse (ed), Engineering Hydraulics, John Wiley & Sons, Inc. New York, NY.
Kennedy, E. (1984). Discharge ratings at gaging stations: US Geological Survey Techniques of Water-Resources Investigations, book 3, chap. A10, 59.
Kozák, M. (1977). A szabadfelszínü nempermanens vízmozgások számítása digitális számítógép felhasználásával. Akadémiai Kiadó, Budapest, Hungary (in Hungarian)
Levesque, V. A. and Oberg, K. A. (2012). Computing discharge using the index velocity method: US Department of the Interior, US Geological Survey.
Lighthill, M.J. and Whitham, G.B. (1955). On Kinematic Wave: I – Flood movement in long rivers, Proc. Royal Society (London), (A), 229 (1178), https://doi.org/10.1098/rspa.1955.0088, p. 281
Manfreda, S., Miglino, D., Saddi, K.C., Jomaa, S., Eltner, A., Perks, M., Peña-Haro, S., Bogaard, T., van Emmerik, T.H.M., Mariani, S. Maddock, I., Tauro, F., Grimaldi, S., Zeng, Y., Gonçalves, G., Strelnikova, D., Bussettini, M., Marchetti, G., Lastoria, B., Su, Z and Rode, M. (2024) Advancing river monitoring using image-based techniques: challenges and opportunities, Hydrological Sciences Journal., 69 (6), DOI: 10.1080/02626667.2024.2333846, 657-677.
Moussa, R., & Bocquillon, C. (1996). Criteria for the choice of flood-routing methods in natural channels. *Journal of Hydrology*, *186*(1-4), 1-30, DOI: 10.1016/S0022-1694(96)03045-4.
Mrokowska, M., Rowinski, P., and Kalinowska, M. (2015a). A methodological approach of estimating resistance to flow under unsteady flow conditions. Hydrology & Earth System Sciences, 19(10).
Mrokowska, M.M., Rowinski, P.M. and Kalinowska, M.B. (2015b) Evaluation of friction velocity in unsteady flow experiments, Journal of Hydraulic Research, 53(5), DOI: 10.1080/00221686.2015.1072853, pp. 659-669,
Muste, M., Lyn, D. A., Admiraal, D., Ettema, R., Nikora, V., & Garcia, M. H. (2017). *Experimental hydraulics: Methods, instrumentation, data processing and management: Volume I: Fundamentals and methods*. CRC Press, DOI: 10.4324/9781315158839.
Muste, M., Bacotiu, C. and Thomas, D. (2019). Evaluation of the slope-area method for continuous streamflow monitoring. Paper presented at the Proceedings of the 38th World Congress, Panama City, Panama
Muste, M., Lee, K., Kim, D., Bacotiu, C., Rojas Oliveros, M., Cheng, Z. and Quintero, F. (2020). “Revisiting Hysteresis of Flow Variables in Monitoring Unsteady Streamflows” State-of-the-art Paper Series, Journal of Hydraulic Research; 58(6), pp. 867-887, https://doi.org/10.1080/00221686.2020.1786742
Muste, M., Kim, D. and Kim, K. (2022). A flood-crest forecast prototype for river floods using only in-stream measurements, Communications Earth & Environment, https://doi.org/10.1038/s43247-022-00402-z
Muste, M., Kim, K., Kim, D. and Fleit G. (2025). Decoding the hysteretic behavior of hydraulic variables in lowland rivers with multivariate monitoring approaches, Hydrological Processes, Special Issue on “Hydrological processes in lowlands and plains”. https://doi.org/10.1002/hyp.70008, 21 p.
Nardi, F., Cudennec, C., Abrate, T., Allouch, C., Annis, A., Assumpção, T., … Grimaldi, S. (2021). Citizens AND HYdrology (CANDHY): conceptualizing a transdisciplinary framework for citizen science addressing hydrological challenges. Hydrological Sciences Journal., 67(16), https://doi.org/10.1080/02626667.2020.1849707, pp. 2534–2551.
Noto, S., Tauro, F., Petroselli, A., Apollonio, C., Botter, G., and Grimaldi, S. (2022). Low-cost stage-camera system for continuous water-level monitoring in ephemeral streams, Hydrological Sciences Journal., 67, doi.org/10.1080/02626667.2022.2079415, pp. 1439–1448.

NOAA (2023). Novel physically-based streamflow monitoring methodology, National Oceanic and Atmospheric Administration (NOAA) project NA22NWS4320003awarded to the Cooperative Institute for Research on Hydrology (CIROH) through the NOAA Cooperative Agreement with The University of Alabama.

NSF (2022). Novel integration of direct measurements with numerical models for real-time estimation and forecasting of streamflow response to cyclical processes, National Science Foundation- EAR-HS award 2139649.

Paul, J.D., Buytaert, W and Sah, N. (2020). A technical evaluation of lidar-based measurements of river water levels, Water Resources Research, 56, e2019WR026810, doi.org/10/1029/2019WR026810

Pereira, T.S.R.; de Carvalho, T.P.; Mendes, T.A.; Formiga, K.T.M. (2022). Evaluation of Water Level in Flowing Channels Using Ultrasonic Sensors. Sustainability 2022, 14, doi.org/10.3390/su14095512, p. 5512.

Perumal., M., T. Moramarco, B. Sahoo, and S. Barbetta (2007), A methodology for discharge estimation and rating curve development at ungauged river sites, Water Resour. Res., 43, W02412, doi:10.1029/2005WR004609.

Rantz, S.E., et al., (1982). ”Measurement and Computation of Streamflow: Volume 2. Computation of Discharge,” Water-Supply Paper 2175, U.S. Geological Survey, pp. 285-631

Rode, M., Wade, A.J., Cohen, M., Hensley, R.T., Bowes, M.J., Kirchner, J.S., Arhonditsis, G.B., Jordan, P., Krovang, B., Halliday, S.J., Skeffington, R.A., Rozeneijer, J.V., Aubert, A. H., Rinle, K. and Jomaa, S. (2016). Sensors in the stream: the high-frequency wave of the present, Environmental Science & Technology, 50(19) doi:10.1021/acs.est.6b02155, pp. 10297–10307.

Schmidt, A.R., (2002). Analysis of stage-discharge relations for open-channel flows and their associated uncertainties, Ph.D. Thesis, University of Illinois at Urbana-Champaign, Department of Civil and Environmental Engineering, 349 p.

Schumann, G., G. Di Baldassarre, D. Alsdorf, and P. D. Bates (2010), Near real-time flood wave approximation on large rivers from space: Application to the River Po, Italy, Water Resour. Res., 46, W05601, doi:10.1029/2008WR007672.

Sergeant, C.J. and Nagorski, S. (2015). The implications of monitoring frequency for describing riverine water quality regimes. River Research and Applications, 31(5), doi:10.1002/rra.2767, pp. 602–610.

Smith, C.F. (2003). Continuous slope-area method for determining stream discharge , In Sustainability Issues of Arizona’s regional watersheds, Arizona Hydrological Society, Proceedings of the 16th Annual Symposium, September 17–20, 2003, Mesa, Arizona, pp. 155–156.

Smith, C.F., Cordova, J.T., and Wiele, S.M. (2010). The continuous slope-area method for computing event hydrographs: U.S. Geological Survey Scientific Investigations Report 2010-5241, 37 p.

Stewart, A. M., Callegary, J. B., Smith, C. F., Gupta, H. V., Leenhouts, J. M., & Fritzinger, R. A. (2012). Use of the continuous slope-area method to estimate runoff in a network of ephemeral channels, southeast Arizona, USA, Journal of Hydrology, 472, pp. 148-158.

Neeson, T.M., Gorman, A.M., Whiting, P.J. and Koonce, J.F. (2008). (2008) Factors affecting accuracy of stream channel slope estimates derived from Geographical Information Systems, North American Journal of Fisheries Management, 28 (3), DOI:10.1577/M05-127.1, pp. 722-732.

Triki, A. (2014). Resonance of free-surface waves provoked by floodgate maneuvers. Journal of Hydrologic Engineering, 19(6), 1124-1130.

Triki, A. (2017). Further investigation on the resonance of free-surface waves provoked by floodgate maneuvers: Negative surge waves. Ocean Engineering, 133, 133-141.

Turnipseed, D. P. and Sauer, V. B. (2010). Discharge measurements at gaging stations, Tech. Rep. 3-A8, U.S. Geological Survey, doi.org/10.3133/tm3A8, iSSN: 2328-7055.

USACE, 2022. Upper Mississippi River Phase III Flood Risk Management Existing Conditions Hydraulic Model Documentation Report. https://www.mvr.usace.army.mil/Portals/48/docs/FRM/UMR%20Hydraulic%20Model%20Phase%20III%20-%20Report.pdf

Wickert, A. D., Sandell, C. T., Schulz, B., and Ng, G.-H. C. (2019). Open-source Arduino-compatible data loggers designed for field research, Hydrol. Earth Syst. Sci., 23, doi.org/10.5194/hess-23-2065-2019.

Wickert, A. D., Jones, J. C., and Ng, G.-H. C. (2024). A double-Manning approach to compute robust rating curves and hydraulic geometries, EGUsphere [preprint], doi.org/10.5194/egusphere-2023-3118.